Quaternary Geochronology 50 (2019) 109–125

Contents lists available at ScienceDirect

Quaternary Geochronology

journal homepage: www.elsevier.com/locate/quageo

In situ ^{10}Be production-rate calibration from a ^{14}C-dated late-glacial moraine belt in Rannoch Moor, central Scottish Highlands

Aaron E. Putnam[a,b,*], Gordon R.M. Bromley[c], Kurt Rademaker[d], Joerg M. Schaefer[b]

[a] *School of Earth and Climate Sciences and Climate Change Institute, University of Maine, Orono, ME, 04473, USA*
[b] *Lamont-Doherty Earth Observatory and Department of Earth and Environmental Sciences, Columbia University, Palisades, NY, 10964, USA*
[c] *School of Geography and Archaeology, Palaeoenvironmental Research Unit, National University of Ireland, Galway, Ireland*
[d] *Department of Anthropology, Michigan State University, East Lansing, MI, 48824, USA*

ARTICLE INFO

Keywords:
Cosmogenic nuclide
Moraine
Younger Dryas
Radiocarbon

ABSTRACT

An objective of terrestrial *in situ* cosmogenic nuclide research is to obtain precise and accurate production-rate estimates on the basis of geological calibration sites from a diverse range of latitudes and altitudes. However, a challenge has been to establish production rates on the basis of landforms for which independent ages have been determined directly using absolute isotopic dating techniques. Here we present a ^{10}Be production-rate calibration from a recessional moraine belt located in Rannoch Moor, central Scottish Highlands (56.63°N, 4.77°W; ~310–330 m a.s.l.). This moraine belt was deposited at the margin of the disintegrating late-glacial West Highland ice field (WHIF) during the final stages of deglaciation. Minimum-limiting ^{14}C dates on macrofossils of the earliest terrestrial vegetation to arrive on the landscape place the timing of moraine abandonment, and hence exposure of morainal boulder surfaces to the cosmic-ray flux, to no later than 12,480 ± 100 calendar years before C.E. 1950 (cal yrs BP). Maximum-limiting ^{14}C dates on marine shells incorporated into basal tills deposited during expansion of the WHIF to its full late-glacial extent place the onset of deglaciation, and thus deglaciation of Rannoch Moor, to no earlier than 12,700 ± 100 cal yrs BP. After removal of a single high-concentration outlier, surface ^{10}Be concentrations of 11 boulders rooted in two sub-parallel moraine ridges exhibit a high degree of internal consistency and affords an arithmetic mean of 6.93 ± 0.24 [x10^4] atoms g^{-1} (1σ). This data set yields a site-specific ^{10}Be production rate of 5.50 ± 0.18 at g^{-1} yr^{-1}, based on the midpoint age 12,590 ± 140 cal yrs BP of the bracketing ^{14}C chronology. Transforming this result to sea-level/high-latitude (SLHL) neutron-spallation ^{10}Be production-rate values using Version 3 of the University of Washington (UW) Online Production-Rate Calculator yields upper and lower bounds, and a mid-point rate. Maximum-limiting SLHL ^{10}Be production rates, based on minimum-limiting ^{14}C age control, are 3.95 ± 0.11 (2.7%) at g^{-1} yr^{-1} for the commonly used 'Lm' and 'St' scaling protocols. The corresponding (non-dimensional) correction factor for a reference production rate determined by the LSDn scaling model is 0.79 ± 0.02 (2.7%). Minimum-limiting SLHL reference ^{10}Be production rates, based on maximum-limiting ^{14}C age control, are 3.88 ± 0.11 (2.7%) at g^{-1} yr^{-1} (St) and 3.89 ± 0.11 (2.7%) at g^{-1} yr^{-1} (Lm). The corresponding correction factor for LSDn scaling is 0.77 ± 0.02 (2.7%). SLHL reference production-rate values based on a midpoint age of 12,590 ± 140 yrs are 3.91 ± 0.11 (2.8%) at g^{-1} yr^{-1} (St) and 3.92 ± 0.11 (2.8%) at g^{-1} yr^{-1} (Lm). The corresponding correction factor for LSDn scaling is 0.78 ± 0.02. The production-rate calibration data set presented here for Scotland yields SLHL values that agree with those determined from calibration data sets based on directly dated landforms from northeastern North America, the Arctic, the Swiss Alps, the Southern Hemisphere middle latitudes, and from the high tropical Andes. We suggest that this production-rate calibration data set from the central Scottish Highlands, used together with the UW online calculators, will produce accurate ^{10}Be surface-exposure ages in the British Isles.

1. Introduction

Knowing the rates at which cosmogenic nuclides are produced *in situ* beneath exposed rock surfaces is essential for the calculation of surface-exposure ages and erosion rates used in studies of landform chronologies and Earth-surface processes. A challenge remains to improve the precision and accuracy of cosmogenic nuclide production rates for the purpose of developing more accurate surface-exposure

* Corresponding author. 224 Bryand Global Sciences Center, School of Earth and Climate Sciences and Climate Change Institute, University of Maine, Orono, ME, 04473, USA.

E-mail address: aaron.putnam@maine.edu (A.E. Putnam).

https://doi.org/10.1016/j.quageo.2018.11.006
Received 10 August 2018; Received in revised form 16 November 2018; Accepted 19 November 2018
Available online 23 November 2018
1871-1014/

chronologies. A leading approach has been to determine production rates empirically by targeting geological calibration sites in which cosmogenic nuclide concentrations can be measured *in situ* from rock surfaces associated with landforms of independently known age (e.g., Balco et al., 2009; Balco et al., 2008; Borchers et al., 2016; Goehring et al., 2010). Empirically determined site-specific production rates are then scaled to other locations using models that account for spatial changes in nuclide production with atmospheric pressure, geomagnetic latitude (Lal, 1991; Stone, 2000), and, in some cases, temporal variations in the strength of Earth's magnetic field and solar wind (Balco

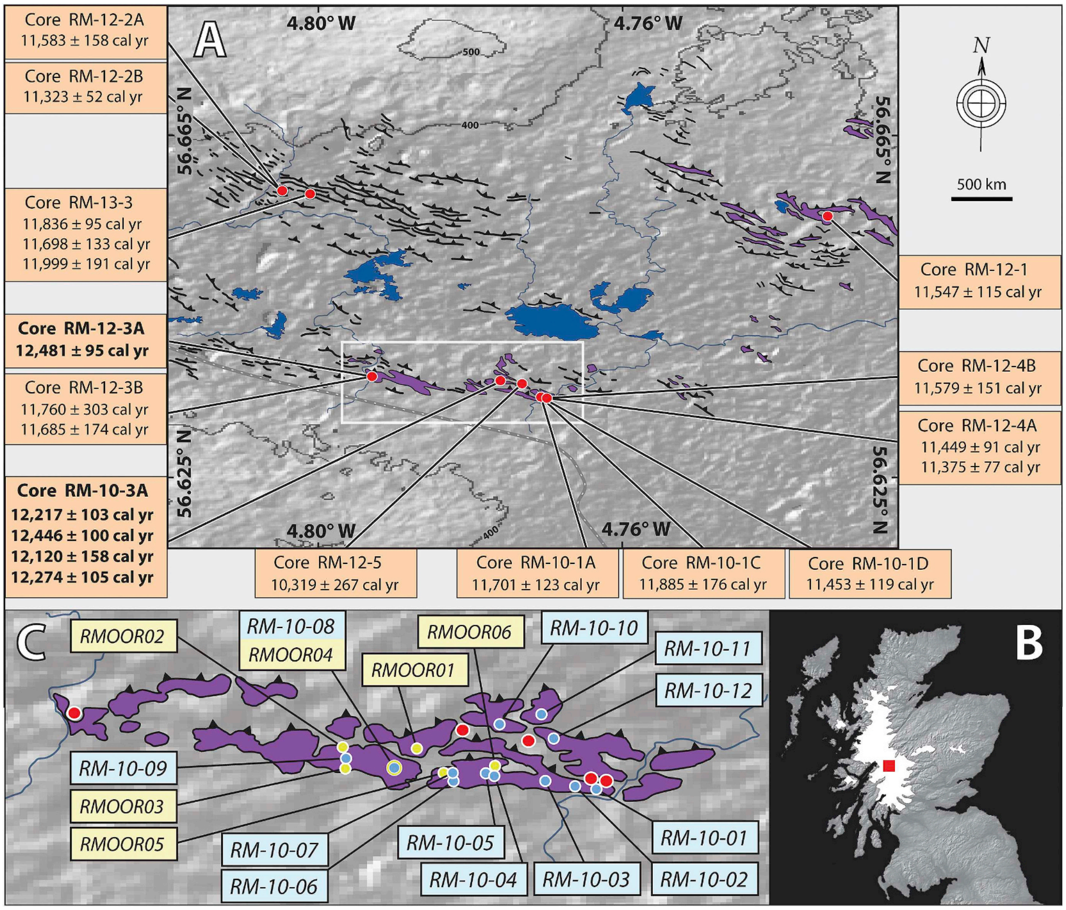

Fig. 1. Geographic and glacial-geomorphic setting of the Rannoch Moor ^{10}Be calibration site. **A)** Distribution of moraine ridges on Rannoch Moor and locations (red circles) of sediment cores, along with respective basal ^{14}C ages. Radiocarbon dates are shown as calibrated ages, with the closest limiting minimum ages for deglaciation in bold. Topographic contours are shown in gray (interval = 100 m). **B)** Position of Rannoch Moor in Scotland and estimated extent of the WHIF. **C)** Zoomed-in view of the Rannoch Moor moraine belt, indicating the locations of boulders sampled for cosmogenic ^{10}Be measurement (blue circles: this study; yellow circles: Small and Fabel (2016b)). Sediment core sites denoted by red circles correspond to those shown in Panel A. Adapted from Fig. 2 in Bromley et al. (2014).

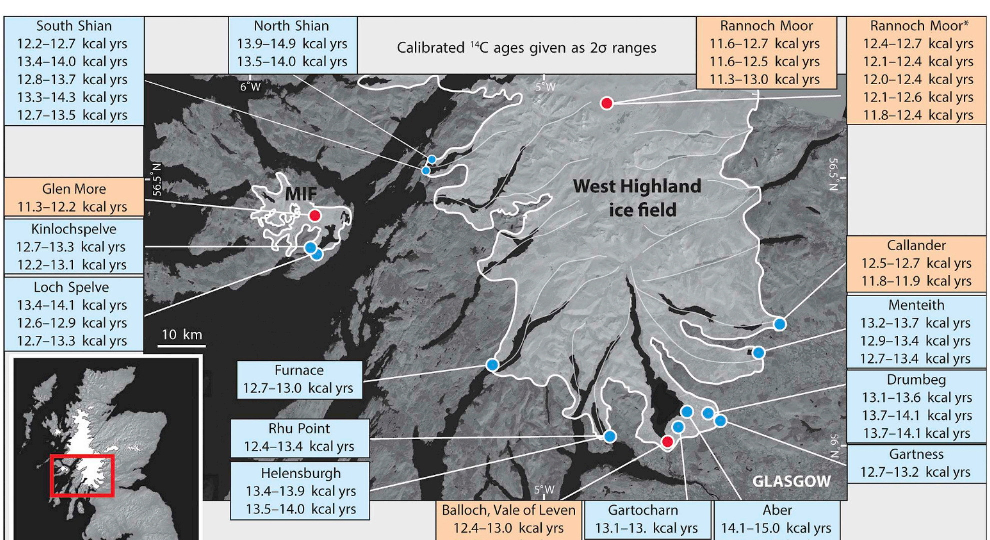

Fig. 2. Former extent of the southern WHIF and the radiocarbon chronology (in kcal yr B.P.) used to bracket its maximum extent. Also shown is the former Mull ice field (MIF). Blue circles represent the locations of maximum-limiting ^{14}C ages, while red circles indicate the locations of minimum-limiting ages. Minimum ages from Rannoch Moor include the five oldest basal ages reported by Bromley et al. (2014) (asterisk) together with those published earlier by Walker and Lowe (1979). Adapted from Fig. 1 of Bromley et al. (2018).

Fig. 3. Panorama of the Rannoch Moor moraine belt. Vantage is to the east. The boulder-mantled sub-parallel moraine ridges are featured in the center of the photograph. Intermorainal depressions were the targets for coring described in Bromley et al. (2014).

et al., 2008; Borchers et al., 2016; Lifton et al., 2005, 2008, 2014; Pigati and Lifton, 2004). Production rates have been conventionally scaled to a nominal value at sea-level and high latitude (SLHL) in order to facilitate comparison among calibration sites in disparate locations (Balco, 2011; Balco et al., 2008, 2009; Borchers et al., 2016; Goehring et al., 2010; Kaplan et al., 2011; Putnam et al., 2010b). A community-wide effort devoted to developing a network of geological calibration sites, distributed across diverse latitudes and altitudes, has improved understanding of cosmogenic nuclide production rates on a global basis and has in turn helped to hone scaling methods (Balco et al., 2008; Borchers et al., 2016; Heyman, 2014; Phillips, 2015; Phillips et al., 2016).

There is particular interest in constraining *in situ* ^{10}Be spallation production rates and scaling protocols. Because of the comparatively uncomplicated production systematics of this relatively long-lived nuclide [e.g., half-life = 1.4 Myrs (Chmeleff et al., 2010; Korschinek et al., 2009; Nishiizumi et al., 2007)] in the abundant mineral quartz, ^{10}Be has become a commonly used geochronological tool. Improvements in the precision of ^{10}Be analyses has led to transformational progress in the development of landform chronologies (Balco, 2011). Challenges remain, however, especially as answers to emerging scientific questions demand ever-greater chronological accuracy. For example, dispersion among existing SLHL ^{10}Be production-rate estimates indicates remaining uncertainties attending the geological calibration sites themselves and lingering imperfections in scaling models (Borchers et al., 2016; Phillips et al., 2016). This dispersion serves as a source of systematic uncertainty for landform chronologies, especially for regions with no nearby calibration sites. Furthermore, of the available published geological ^{10}Be calibration sites, relatively few are anchored by landforms underpinned directly, at the site, by absolute chronologies. Many sites instead depend upon indirect associations among target landforms and other distal paleoclimatic/stratigraphic signatures (e.g., Ballantyne and Stone, 2012; Borchers et al., 2016; Goehring et al., 2012; Small and Fabel, 2015; Stroeven et al., 2015). Any incorrect assumptions incorporated into production-rates calibrated in this way could accidentally mislead attempts at evaluating and improving scaling protocols (Phillips et al., 2016). Further development of geological ^{10}Be production-rate calibration sites based upon landforms with direct and absolute-dated chronological constraints will help to sharpen empirical estimates of cosmogenic nuclide production rates and aid in improving scaling protocols.

Here, we present a ^{10}Be production-rate calibration data set based on a ^{14}C-dated late-glacial moraine belt located at Rannoch Moor, central Scottish Highlands. Although there are now four published ^{10}Be production-rate calibration sites in Scotland (e.g., Ballantyne and Stone, 2012; Borchers et al., 2016; Small and Fabel, 2015), none is based on landforms that have been directly dated with absolute radiometric techniques (Phillips et al., 2016). Instead, landform ages have been assessed based on assumed correlations to distal biological and/or ice-core-inferred paleoclimatic signatures (Balco et al., 2008; Ballantyne and Stone, 2012; Borchers et al., 2016; Phillips et al., 2016; Stone et al., 1998), or else tentative correlations to distal and undated lacustrine sediments and tephrostratigraphy (Small and Fabel, 2015). Consequently, the reference SLHL production-rate values from these sites exhibit deviation from published production-rate calibration data sets from elsewhere. This has led to the question of whether problems with scaling models, or the calibration sites themselves, are responsible for the discrepancy among Scottish calibration data sets and data sets based on directly dated landforms from father afield (Phillips et al., 2016).

The age of the Rannoch Moor moraine belt is bracketed by maximum- and minimum-limiting ^{14}C ages, and thus affords minimum- and maximum-limiting bounds, respectively, on the regional *in situ* production rate of ^{10}Be. We (1) present a new geological ^{10}Be calibration data set for the central Scottish Highlands; (2) discuss the fit to distal calibration data sets, with implications for available scaling models; (3) evaluate which previously published production-rate estimates would produce ^{10}Be surface-exposure ages that are compatible with the bracketing ^{14}C chronology; and (4) address previously published ^{10}Be data sets from Rannoch Moor in the context of the results presented here.

2. Prior work

Four published calibration data sets exist for the Scottish Highlands. These data are from Coire Mhic Fearchair, Maol Chean Dearg, Corie nan Arr (Ballantyne and Stone, 2012; Borchers et al., 2016), and from Glen Roy (Small and Fabel, 2015). Data from Coire Mhic Fearchair, Maol Chean Dearg, and Corie nan Arr are included in the primary global calibration data set of Borchers et al. (2016).

The three studies at Coire Mhic Fearchair (57.2°N, 5.97°W), Maol

Table 1
^{14}C data. Minimum-limiting and maximum-limiting ages are noted in 'context' column.

Core/Site	AMS no.	Latitude (°)	Longitude (°)	^{14}C age (yrs; ± 1σ)	Calendar age (cal yrs BP)	$\delta^{13}C$	Material dated	Context	Reference	Notes
RM-10-1A	OS-93723	56.6338 N	4.7714 W	10,100 ± 35	11,701 ± 123	−28.0	Beetle	Minimum	Bromley et al. (2014)	Ages in this group are all from samples recovered from the lowermost sediments of Rannoch Moor bogs (Bromley et al., 2014). Asterisks denote replicate samples from respective cores. Bold indicates the 5 oldest samples used to provide minimum ages for deglaciation of Rannoch Moor in the Bromley et al. (2014) paper.
RM-10-1C	OS-84320	56.6338 N	4.7714 W	10,200 ± 80	11,885 ± 176	−22.7	*Pogonatum* sp., unidentified leaf fragments	Minimum	Bromley et al. (2014)	
RM-10-1D	OS-89837	56.6338 N	4.7714 W	9980 ± 50	12,217 ± 103	−24.1	*Sphagnum* sp., *Potamogeton* sp., Betula leaf	Minimum	Bromley et al. (2014)	
RM-10-3A	**OS-99978***	**56.6358 N**	**4.7763 W**	**10,350 ± 40**	**12,217 ± 103**	**−20.0**	***Empetrum* sp. seed, *Pogonatum* sp., unidentified stem**	**Minimum**	Bromley et al. (2014)	
RM-10-3A	**OS-8982***	**56.6358 N**	**4.7763 W**	**10,500 ± 50**	**12,446 ± 100**	**−21.7**	***Sphagnum* sp., *Pogonatum* sp., unidentified leaf fragments**	**Minimum**	Bromley et al. (2014)	
RM-10-3A	**OS-89841***	**56.6358 N**	**4.7763 W**	**10,300 ± 70**	**12,120 ± 158**	**−23.5**	***Chara* sp., *Nitella* sp., *Potamogeton* sp., *Empetrum* sp. seed**	**Minimum**	Bromley et al. (2014)	
RM-10-3A	**OS-99977***	**56.6358 N**	**4.7763 W**	**10,400 ± 45**	**12,274 ± 105**	**−21.5**	***Empetrum* sp. seed, *Pogonatum***	**Minimum**	Bromley et al. (2014)	
RM-12-1	112593	56.6565 N	4.7349 W	10,040 ± 40	11,547 ± 115	NR	*Potamogeton sp.*, *Pogonatum* sp., unidentified stems	Minimum	Bromley et al. (2014)	
RM-12-2A	OS-99684	56.6594 N	4.8039 W	10,050 ± 65	11,583 ± 158	−24.3	*Sphagnum* sp., *Pogonatum* sp., *Potamogeton* sp.	Minimum	Bromley et al. (2014)	
RM-12-2B	112598	56.6594 N	4.8039 W	9945 ± 20	11,332 ± 52	NR	*Rhacomitrium* sp., *Pogonatum* sp., *Empetrum* sp. seed, unidentified bud	Minimum	Bromley et al. (2014)	
RM-12-3A	**OS-99685**	**56.6367 N**	**4.7922 W**	**10,550 ± 65**	**12,481 ± 95**	**−25.7**	***Pogonatum* sp., wood fragment, *Betula* sp. leaf fragment**	**Minimum**	Bromley et al. (2014)	
RM-12-3B	112603*	56.6367 N	4.7922 W	10,120 ± 170	11,760 ± 303	NR	*Pogonatum* sp., *Vaccinium* sp. leaf fragments	Minimum	Bromley et al. (2014)	
RM-12-3B	OS-100115*	56.6367 N	4.7922 W	10,100 ± 70	11,685 ± 174	−19.8	Unidentified leaf fragments	Minimum	Bromley et al. (2014)	
RM-12-4A	112605*	56.6337 N	4.7714 W	9990 ± 20	11,449 ± 91	NR	*Rhacomitrium* sp.	Minimum	Bromley et al. (2014)	
RM-12-4A	112604*	56.6337 N	4.7714 W	9965 ± 20	11,375 ± 77	NR	*Rhacomitrium* sp.	Minimum	Bromley et al. (2014)	
RM-12-4B	OS-99686	56.6337 N	4.7714 W	10,050 ± 60	11,579 ± 151	−26.8	*Rhacomitrium* sp.	Minimum	Bromley et al. (2014)	
RM-12-5	112608	56.6355 N	4.7732 W	9140 ± 180	10,319 ± 267	NR	*Nitella* sp., *Chara* sp., *Betula* sp. seed, *Sphagnum* sp., unidentified stems	Minimum	Bromley et al. (2014)	
RM-13-3	OS-104748*	56.6594 N	4.8039 W	10,150 ± 35	11,836 ± 95	−25.1	*Rhacomitrium* sp.	Minimum	Bromley et al. (2014)	
RM-13-3	OS-104747*	56.6594 N	4.8039 W	10,100 ± 40	11,698 ± 133	−25.0	*Rhacomitrium* sp.	Minimum	Bromley et al. (2014)	
RM-13-3	OS-104746*	56.6594 N	4.8039 W	10,250 ± 85	11,999 ± 191	−23.6	*Rhacomitrium* sp.	Minimum	Bromley et al. (2014)	
Balloch	SRR-1530	56.0034 N	4.5850 W	11,320 ± 130	12,809 ± 246	NR	Barnacles	Minimum	Browne & Graham (1981)	Ages in this group include published marine and terrestrial samples that together afford minimum-limiting age control for the culmination of the WHIF (from Bromley et al., 2018). These data were used to generate the PDF calculation in Bromley et al. (2018). All marine ages converted using Marine13.
Balloch	OS-2078	56.0034 N	4.5850 W	11,050 ± 45	12,598 ± 93	−0.20	*Portlandia arctica* shell	Minimum	Bromley et al. (2018)	
Mollands	HV-5647	56.2334 N	4.2164 W	10,670 ± 85	12,612 ± 78	NR	Gyttja	Minimum	Lowe, 1982	
Mollands	HV-5646	56.2334 N	4.2164 W	10,480 ± 150	12,330 ± 220	NR	Fine detritus peat	Minimum	Lowe, 1982	
Torness	SRR-1797	56.4328 N	5.8246 W	10,170 ± 150	11,829 ± 292	NR	Gyttja	Minimum	Walker & Lowe (1982)	
Rannoch Station 2	BIRM-858	56.6834 N	4.5809 W	10,390 ± 200	12,163 ± 317	−22.0	Gyttja	Minimum	Walker & Lowe (1979)	
K2	BIRM-722	56.6594 N	4.8039 W	10,290 ± 180	12,031 ± 321	NR	*Rhacomitrium* sp.	Minimum	Lowe and Walker, 1976	
K2	BIRM-723	56.6594 N	4.8039 W	10,520 ± 330	12,245 ± 442	−22.4	Gyttja	Minimum	Lowe and Walker, 1976	
Kinlochspelve	AA15940	56.3687 N	5.7981 W	11,621 ± 117	13,096 ± 257	1.9	*Astarte elliptica*	Maximum	Bromley et al. (2018)	Ages in this population include published marine samples that together afford maximum-limiting age control for the culmination of the WHIF (from Bromley et al., 2018). These data were used to generate the PDF in Bromley et al. (2018). All marine ages converted using Marine13.
Kinlochspelve	I-5308	56.3687 N	5.7981 W	11,330 ± 170	12,830 ± 315	NR	Unidentified shell fragments	Maximum	Gray & Brooks (1972)	
Loch Spelve	AA15941	56.3650 N	5.7856 W	12,167 ± 130	13,625 ± 281	1.6	*Arctica islandica*	Maximum	Bromley et al. (2018)	
Loch Spelve	AA15942	56.3650 N	5.7856 W	11,352 ± 92	12,824 ± 201	2.2	*Astarte elliptica*	Maximum	Bromley et al. (2018)	
Loch Spelve	AA15943	56.3650 N	5.7856 W	11,668 ± 86	13,154 ± 202	0.1	*Nuculana pernula*	Maximum	Bromley et al. (2018)	
South Shian	AA15945	56.5252 N	5.4018 W	11,192 ± 78	12,688 ± 141	1.9	*Astarte elliptica*	Maximum	Bromley et al. (2018)	
South Shian	AA15946	56.5252 N	5.4018 W	12,157 ± 120	13,614 ± 262	2.5	*Arctica islandica*	Maximum	Bromley et al. (2018)	
South Shian	IGS C14/16	56.5252 N	5.4018 W	11,930 ± 210	13,400 ± 450	NR	*Chlamys islandicus*	Maximum	Peacock (1971)	
South Shian	IGS C14/17	56.5252 N	5.4018 W	12,205 ± 180	13,669 ± 375	NR	*Astarte elliptica*	Maximum	Peacock (1971)	
South Shian	IGS C14/18	56.5252 N	5.4018 W	11,830 ± 220	13,295 ± 468	NR	Unidentified shell fragments	Maximum	Peacock (1971)	
North Shian	AA15947	56.5345 N	5.3895 W	12,700 ± 116	14,326 ± 477	2.7	*Arctica islandica*	Maximum	Bromley et al. (2018)	
North Shian	AA15948	56.5345 N	5.3895 W	12,179 ± 85	13,632 ± 206	1.3	Unidentified shell fragments	Maximum	Bromley et al. (2018)	
Furnace	OS-2077	56.1502 N	5.1882 W	11,450 ± 45	12,914 ± 206	1.4	Unidentified shell fragments	Maximum	Bromley et al. (2018)	
Gartocharn	AA15951	56.0392 N	4.5290 W	12,021 ± 89	13,472 ± 202	0.1	*Astarte elliptica*	Maximum	Bromley et al. (2018)	

(*continued on next page*)

Table 1 (*continued*)

Core/Site	AMS no.	Latitude (°)	Longitude (°)	^{14}C age (yrs; ± 1σ)	Calendar age (cal yrs BP)	$\delta^{13}C$	Material dated	Context	Reference	Notes
Aber	AA15949	56.0564 N	4.5280 W	12,816 ± 86	14,518 ± 421	0.8	Unidentified shell fragments	Maximum	Bromley et al. (2018)	
Aber	AA15950	56.0564 N	4.5280 W	12,528 ± 94	14,014 ± 250	0.6	Unidentified shell fragments	Maximum	Bromley et al. (2018)	
Drumbeg	AA15952	56.0571 N	4.4378 W	12,021 ± 89	13,472 ± 202	−1.1	Unidentified shell fragments	Maximum	Bromley et al. (2018)	
Drumbeg	OS-2076	56.0571 N	4.4378 W	12,250 ± 50	13,713 ± 167	3.2	*Chlamys islandicus*	Maximum	Bromley et al. (2018)	
Gartness	AA15953	56.0401 N	4.4139 W	11,593 ± 79	13,072 ± 202	0.8	Unidentified shell fragments	Maximum	Bromley et al. (2018)	
Gartness	OS-133096	56.0401 N	4.4139 W	12,650 ± 35	14,142 ± 150	0.6	*Astarte borealis*	Maximum	Bromley et al. (2018)	
Menteith	AA15938	56.1717 N	4.2742 W	12,058 ± 89	13,511 ± 206	0.8	*Mytilus edulis* fragments	Maximum	Bromley et al. (2018)	
Menteith	AA15939	56.1717 N	4.2742 W	11,843 ± 88	13,312 ± 203	3.0	Unidentified shell fragments	Maximum	Bromley et al. (2018)	
Menteith	I-2234	56.1717 N	4.2742 W	11,800 ± 170	13,265 ± 371	NR	Unreported	Maximum	Sissons (1967)	
Drymen	I-2235	56.0607 N	4.4380 W	11,700 ± 170	13,165 ± 347	NR	Unreported	Maximum	Sissons (1967)	
Rhu Point	HAR-931	56.0163 N	4.7858 W	11,520 ± 250	13,001 ± 453	NR	Unreported	Maximum	Rose (1980)	
Helensburgh	SRR-2006	56.0092 N	4.7024 W	12,110 ± 60	13,559 ± 167	NR	*Arctica islandica*	Maximum	Browne et al. (1983)	
Helensburgh	NR	56.0092 N	4.7024 W	12,190 ± 60	13,642 ± 172	NR	*Arctica islandica*	Maximum	Browne et al. (1983)	

Chean Dearg (57.49°N, 5.45°W), and Corie nan Arr (57.4°N, 5.6°W) are all based on ^{10}Be concentrations measured from erratic boulders resting on the floors of glacial corries, inboard of late-glacial moraine limits, in the western Scottish Highlands (Ballantyne and Stone, 2012). For production-rate calibration purposes, erratic boulders in each of these settings were assigned an 'independent' age of 11,700 ± 300 yrs. This assigned independent age was not determined by direct dating of the calibration landforms, but was instead tied to the assumption that rapid changes in mean-annual air temperatures at the end of the Younger Dryas stadial, recorded in $\delta^{18}O$ data derived from Greenland ice cores and paleo-ecological records in Britain, applied to glacier changes in Scotland (Ballantyne and Stone, 2012).

We note that we have reservations about the underlying assumptions used in these previous calibration studies that (i) Scottish glacier-margin fluctuations should share the same signature as isotopic fluctuations recorded in Greenlandic ice, or else by paleo-ecological proxies, and (ii) that undated glacial geomorphologic landforms can be matched to these isotopic signatures. Recent studies have shown that air-temperatures recorded in Greenlandic ice-core proxies are dominated by winter conditions (Broecker, 2006; Buizert et al., 2014; Denton et al., 2005), whereas mountain glaciers are dominantly driven by ablation-season (i.e., summer) temperatures (e.g., Mackintosh et al., 2017; Zemp et al., 2015; Rupper and Roe, 2008; Oerlemans, 2005). Observation of a significant mismatch between the magnitudes of reconstructed glacier snowline elvatons and ice-core derived temperatures during late-glacial time led to the hypothesis that North Atlantic stadials, such as the Younger Dryas (12,900–11,600 yrs ago), were characterized by extreme seasonality (Denton et al., 2005). By this hypothesis, North Atlantic climate during the Younger Dryas involved mild summers relative to hyper-cold winters on account of winter sea-ice expansion over the freshened surface of the northern North Atlantic (Denton et al., 2005; Schenk et al., 2018). In light of this recent progress in understanding ancient water isotope changes in Greenland snow (and related re-interpretations of paleotemperature records from Greenland ice cores), we feel that 'independent' age assignments tied indirectly to paleoclimate proxies in these earlier production-rate studies should be reevaluated. As we demonstrate below, applying previously published Scottish production-rate calibration datasets (that are tied to the Greenland ice-core chronology) to the Rannoch Moor ^{10}Be data from this study results in ^{10}Be surface-exposure ages that are too young with respect to the limiting radiocarbon chronology.

The fourth ^{10}Be production-rate calibration data set from Glen Roy, presented by Small and Fabel (2015), is based on four ^{10}Be measurements from a 325-m a.s.l. wave-cut bedrock bench associated with the classic 'Parallel Roads of Glen Roy' (56.99°N, 4.68°W). The wave-cut shoreline was developed at the edge of a proglacial lake that was dammed by the Spean paleoglacier at the eastern margin of the WHIF during late-glacial time (Sissons, 1978). Small and Fabel (2015) considered various nominal ages between 11,562 ± 422 and 12,013 ± 267 yrs for when the 325-m bench was exposed to the cosmic-ray flux, with 12,013 ± 267 yrs deemed the most likely. Thus an 'independent' age of 12,013 ± 267 yrs has been assigned to the data set available online from the ICE-D production-rate calibration database (Balco, 2018). These age assignments are based on the assumption that the 325-m shoreline was developed coevally with the deposition of varved lacustrine sediments preserved in the Loch Laggan East site – in a different glacier valley approximately 25 km east of Glen Roy – in which a tephra layer is preserved (MacLeod et al., 2015). Critical to this independent age assignation is the correlation of that tephra layer with the Vedde Ash (12,121 ± 114 yrs; Rasmussen et al., 2006). However, this correlation has not been verified by geochemical analysis of the tephra, for which there was insufficient material (MacLeod et al., 2015), nor by radiometric dating of the sediments (Palmer et al., 2010).

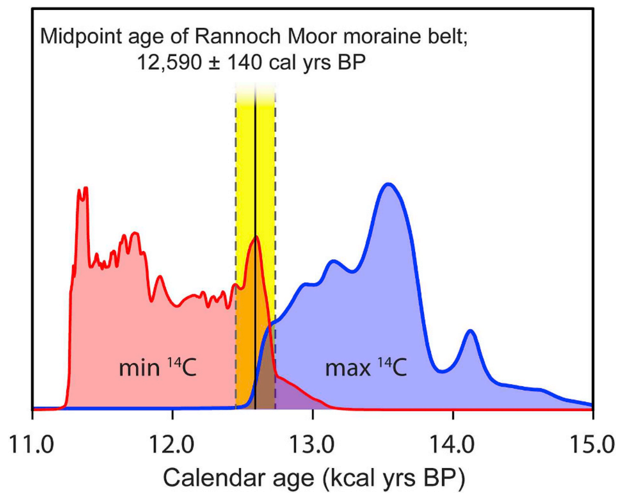

Fig. 4. Probability distribution functions for minimum- and maximum-limiting ^{14}C populations, converted to calendar years, bracketing the latest culmination of the WHIF. The most probable age for the maximum extent of the WHIF, which serves as a maximum age for the Rannoch Moor moraines in this study, was calculated using a PDF (not shown) of the interval between the two populations. Vertical black line and yellow shading represent the mean age and 1σ uncertainty, respectively, of the Rannoch Moor beryllium ages (n = 11) calculated with our production rate. Adapted from Fig. 3 of Bromley et al. (2018).

3. Rannoch Moor calibration site: setting and basis for independent age assignment

Rannoch Moor (56.63°N, 4.77°W; ~310–330 m a.s.l.; Fig. 1) is an extensive, peat-covered moorland surrounded by high-relief glacially-molded peaks of the southern Grampian Mountains. By most glaciological reconstructions, Rannoch Moor lay near the center of the West Highland ice field (WHIF) during late-glacial time and was likely one of the last lowland regions in Scotland to become deglaciated (Figs. 1 and 2; Golledge, 2010; Golledge et al., 2007; Lowe and Walker, 1976; Sissons, 1976). The landscape of Rannoch Moor is characterized by ground moraine and till-mantled ice-scoured bedrock, and features a belt of semi-parallel, discontinuous moraine ridges that were constructed along the margin of the diminished WHIF just prior to its final deterioration (Fig. 3). We selected Rannoch Moor as a production-rate calibration site for the following reasons. First, moraine ridges of Rannoch Moor feature numerous large, rounded, embedded, quartz-rich granitoid boulders that are well-suited for measuring the amount of *in situ* cosmogenic ^{10}Be production since the time at which the boulders were first exposed to the cosmic-ray flux. Second, the timing of deglaciation of this landscape has been determined by ^{14}C dating of plant macrofossils recovered from the basal sediment of intermorainal depressions. Third, bracketing ^{14}C ages provide a chronology for ice-marginal landforms that delineate the maximum extent of the WHIF, and thus when Rannoch Moor would have been fully buried by glacial ice. Taken altogether, the boulder-rich landforms of Rannoch Moor are well bracketed both by maximum- and minimum-limiting ^{14}C ages, and therefore meet the criteria for accurate production-rate determination on the basis of landforms with direct age control (Phillips et al., 2016).

3.1. Limiting ^{14}C age control for the construction of the Rannoch Moor moraine belt

3.1.1. ^{14}C chronology for the full-bodied WHIF – maximum age control on the Rannoch Moor moraine belt

Twenty-seven ^{14}C dates on marine macrofossils recovered from 10 exposures in basal tills and terminal moraines of the WHIF afford maximum-limiting age control for expansion of the WHIF to its full late-glacial extent. As detailed in Bromley et al. (2018), the dated macrofossils consist of the shells of marine organisms that inhabited the fjords of Scotland's Atlantic coast following the retreat of the British ice sheet. The shells and seafloor sediments were subsequently incorporated into the basal sediments of tidal outlet glaciers during the advance of the WHIF and neighboring Mull ice field, and deposited in terminal moraines and till sheets (Fig. 2; Bromley et al., 2018). ^{14}C ages of shell remains range from 11,190 ± 80 to 12,820 ± 90 ^{14}C yrs ago and convert to a full 2σ age range of 12,600 to 15,000 cal yrs BP (i.e., before the year C.E. 1950) using the MARINE13 radiocarbon calibration curve (Reimer et al., 2013). The choice of an alternative time-dependent marine-^{14}C curve reconstructed for late-glacial time from Norway (Bondevik et al., 2006) yields a similar calibrated age range (2σ) of 12,400 to 14,600 cal yrs BP for the whole data set (Bromley et al., 2018). Because these ^{14}C dates are on marine shells incorporated into WHIF tills, they constitute maximum-limiting ages for (i) the advance of the ice field to its outer moraines, (ii) the subsequent recession of the WHIF margin towards the central Scottish Highlands and Rannoch Moor, (iii) construction of the Rannoch Moor moraine ridges, and (iv) the final stage of deglaciation of WHIF.

Two additional ^{14}C ages on shells recovered from marine sediments at the Balloch borehole site (Fig. 2), Vale of Leven, and located just inboard of the terminal moraine of the Lomond piedmont glacier (a southern outlet of the WHIF), afford stratigraphically consistent minimum-limiting ages of 11,050 ± 45 and 11,320 ± 130 ^{14}C yrs BP for the construction of, and initial recession from, that late-glacial limit (Bromley et al., 2018). These ages convert to 2σ calibrated age ranges of 12,507–12,692 and 12,595–13,087 cal yrs BP, respectively, using the Marine13 calibration curve. Bromley et al. (2018) compiled these minimum-limiting ^{14}C ages from the Balloch borehole and Rannoch Moor, along with previously published minimum ages [Figs. 1 and 2, Table 1 (this study), and Table S2 of Bromley et al., 2018), to produce a minimum-limiting population for the culmination of the WHIF. Together with the population of maximum ages described above (Fig. 2, Table 1; and Table 1 of Bromley et al., 2018), Bromley et al. (2018) then used a probability distribution function of the interval between the two bracketing ^{14}C populations to calculate the most probable age (12,700 ± 100 cal yrs BP) for the culmination of the late-glacial maximum of the WHIF. Further details of this type of statistical treatment are described in Kelly et al. (2015). For the purposes of this study, the estimate of 12,700 ± 100 cal yrs BP for the culmination of the WHIF provides a maximum age for construction of the Rannoch Moor moraines.

3.1.2. Minimum ^{14}C chronology for construction of the Rannoch Moor moraine belt

Basal ^{14}C dates from 13 sediment cores extracted from moraine-dammed basins on Rannoch Moor provide minimum-limiting age control for the Rannoch Moor moraine belt. Stratigraphically, these bog-filled basins are located both amongst and proximal to the moraine ridges sampled for ^{10}Be (Fig. 1). As detailed by Bromley et al. (2014), ^{14}C ages are on fragments of predominantly terrestrial plants (Table 1) that colonized Rannoch Moor following deglaciation and which were subsequently incorporated into basal lake sediments. The potentially complicating influence of hardwater effects and/or contamination by 'old' carbon is considered minimal due to (i) the primarily terrestrial nature of the samples and (ii) removal of any adhering sediment during preparation (see Bromley et al., 2016). Twenty basal ^{14}C ages from the 13 cores range from 9140 ± 180 to 10,550 ± 65 ^{14}C yrs BP, corresponding to a 2σ calibrated (IntCal13; Reimer et al., 2013) range of 9701–12,648 cal yrs BP for the full data set (Table 1; Bromley et al., 2014). Here, adhering to the principles of stratigraphy (e.g., Strelin et al., 2011), we use the oldest, and thus closest, minimum-limiting ^{14}C age for deglaciation of Rannoch Moor (sample OS-99685 from core RM-12-3A; 12,480 ± 100 cal yrs BP calibrated age) for determining the local production rate. Reinforcing this ^{14}C measurement, and thus its suitability for bracketing the Rannoch Moor moraine, we note that this

Fig. 5. Photographs of boulders in the Rannoch Moor field area selected for ^{10}Be sample collection. Sample information is given in Table 2.

single age determination aligns closely with the next-youngest ages in the data set reported by Bromley et al. (2014). Specifically, four statistically indistinguishable ^{14}C ages from core RM-10-3A provide an earliest probable age of 12,490 cal yrs BP for plant growth (and thus deglaciation) based on the 90% confidence interval of their summed probability (see Bromley et al., 2014). The high degree of internal consistency among these five oldest ^{14}C ages, therefore, supports our model that Rannoch Moor was ice free by 12,480 ± 100 cal yrs BP. All ^{14}C sample details are given in Table 1.

3.1.3. *Midpoint age for construction of Rannoch Moor moraines*

Based on the statistical assessment of maximum- and minimum-limiting ^{14}C ages presented by Bromley et al. (2018), we take their most probable age of 12,700 ± 100 cal yrs BP (see Section 3.1.1, above) for the culmination of the full late-glacial WHIF (Bromley et al., 2018) as a maximum-limiting age for the construction of the Rannoch Moor moraine belt. We then take the single oldest age of the Rannoch Moor ^{14}C data set (Bromley et al., 2014) to provide the closest minimum-limiting age of 12,480 ± 100 cal yrs BP for the construction of the Rannoch Moor moraine belt. From the bracketing ^{14}C ages, we take a midpoint value of 12,590 ± 140 cal yrs BP to represent a likely age of exposure of the Rannoch Moor moraine belt (Fig. 4). The uncertainty of this midpoint rate is determined by propagating in quadrature the uncertainties for the respective maximum and minimum age bounds. We note that this uncertainty is slightly greater than the range of the maximum- and minimum-limiting ages. Taken together with ^{10}Be concentrations measured in the surfaces of embedded glacial boulders, these limits and corresponding midpoint for the age of the Rannoch Moor moraine belt provide the basis for production-rate calibration, described below.

4. Methods

Our field and laboratory procedures for obtaining *in situ* ^{10}Be concentrations for production-rate determination followed those reported in Schaefer et al. (2009), Putnam et al. (2010b) and Kaplan et al. (2011), and are described online at http://www.ldeo.columbia.edu/tcn. Methods for developing the ^{14}C chronology of the WHIF and Rannoch Moor deglaciation are reported in Bromley et al. (2018, 2014).

4.1. *Field methods*

Samples were collected for ^{10}Be analysis in April of C.E. 2010. We targeted for sampling the surfaces of boulders rooted in discontinuous ridge segments of the Rannoch Moor moraine belt (Fig. 3). Nine ^{10}Be samples (RM-10-01 to 09) are from the outermost moraine ridge of this

Table 2
Rannoch Moor boulder sample details and ^{10}Be data.

CAMS laboratory no.	Sample ID	Latitude (°)	Longitude (°)	Elevation (m a.s.l.)	Boulder size (L x W x H) (cm)	Sample Thickness (cm)	Shielding corr.	Quartz weight (g)	Carrier added (g)	Carrier conc. (ppm)[a]	^{10}Be/^{9}Be ± 1σ (10^{-14})[b]	[^{10}Be] ± 1σ (10^4 atoms g^{-1})[c]	^{9}Be current (μA)[d]	Blank[e]	AMS Std[f]
BE35521	RM-10-01	56.6334	−4.77118	316	210 x 150 x 68.75	0.93	1.000	25.0222	0.1850	1032	15.179 ± 0.28	7.70 ± 0.15	19.8 (74%)	B3, B4	07KNSTD
BE35522	RM-10-02	56.63338	−4.77133	316	220 x 130 x 86.25	2.23	1.000	20.0469	0.1832	1030	11.041 ± 0.25	6.94 ± 0.16	16.7 (72%)	B1, B2	07KNSTD
BE35523	RM-10-03	56.63369	−4.77312	321	190 x 170 x 87.5	0.75	1.000	20.0032	0.1839	1030	11.312 ± 0.23	7.15 ± 0.15	19.3 (84%)	B1, B2	07KNSTD
BE35524	RM-10-06	56.63377	−4.7766	325	150 x 140 x 101.25	0.67	1.000	15.0040	0.1808	1036	8.758 ± 0.17	7.30 ± 0.14	23.0 (94%)	B5, B6	07KNSTD
BE35525	RM-10-10	56.63592	−4.77492	316	130 x 125 x 98.75	0.66	1.000	14.9393	0.1809	1037	8.214 ± 0.19	6.86 ± 0.16	25.7 (95%)	B7	07KNSTD
BE35526	RM-10-11	56.63633	−4.77294	313	200 x 150 x 98.75	0.94	1.000	15.3106	0.1804	1037	8.389 ± 0.14	6.82 ± 0.11	29.6 (109%)	B7	07KNSTD
BE35527	RM-10-05	56.63385	−4.77544	324	280 x 150 x 50	1.60	1.000	11.1758	0.1837	1045	6.145 ± 0.15	7.03 ± 0.17	12.9 (49%)	B8	07KNSTD
BE35528	RM-10-09	56.63459	−4.78123	326	245 x 190 x 128.75	3.01	0.994	15.0141	0.1834	1045	7.830 ± 0.25	6.66 ± 0.22	21.8 (83%)	B8	07KNSTD
BE35529	RM-10-12	56.6352	−4.77243	316	190 x 130 x 77.5	1.93	1.000	10.8794	0.1825	1045	5.832 ± 0.13	6.81 ± 0.16	20.7 (79%)	B8	07KNSTD
BE35530	RM-10-04	56.63391	−4.77524	324	240 x 125 x 75	2.27	1.000	8.4336	0.1830	1046	4.888 ± 0.12	7.35 ± 0.18	24.7 (103%)	B9	07KNSTD
BE35531	RM-10-07	56.63407	−4.77674	325	155 x 130 x 55	1.41	1.000	10.6886	0.1834	1046	6.032 ± 0.15	7.19 ± 0.19	11.8 (49%)	B9	07KNSTD
BE35532	RM-10-08	56.63414	−4.77869	327	300 x 220 x 120	1.49	1.000	7.8106	0.1834	1046	4.340 ± 0.13	7.06 ± 0.21	20.5 (85%)	B9	07KNSTD

[a] – Carrier concentrations have been corrected for evaporation.
[b] – Boron-corrected ^{10}Be/^{9}Be. Ratios are not corrected for background ^{10}Be detected in procedural blanks.
[c] – Reported [^{10}Be] values have been corrected for background ^{10}Be detected in procedural blanks.
[d] – $^{9}Be^{+3}$ measured after the accelerator. Reported currents are those measured during the first run of each sample. In parentheses is the ratio, given in percent, of each sample current compared with the average of all measured first-run AMS standard currents.
[e] – Procedural blanks used to correct sample concentrations. Blank numbers refer to those given in Table 2. Where two blanks are shown, the average (and propagated error) was used to correct sample concentrations in the respective sample batch.
[f] – AMS standard to which respective ratios and concentrations are referenced. Reported ^{10}Be/^{9}Be ratio for 07KNSTD is 2.85×10^{-12}.

belt, which is immediately outboard of core sites RM-10-1A, RM-10-1C, RM-10-1D, RM-12-4A, RM-12-4B, RM-12-5, and RM-10-3A (Fig. 1; Bromley et al., 2014). Core sites RM-12-2A, RM-12-2B, RM-13-3 and K3 [sampled by Walker and Lowe (1977)] are from a kettle-hole bog within a discontinuous moraine ridge segment also associated with this outboard ridge. Boulders associated with the outermost moraine ridge of the Rannoch Moor belt would have begun their exposure to the cosmic-ray flux prior to the accumulation of plant macrofossils that we targeted for ^{14}C dating.

We also collected four samples for ^{10}Be analysis (RM-10-10 to 13) from a subparallel set of discontinuous moraine ridges located just inside of the outermost ridges; three of these samples were selected for ^{10}Be analysis (RM-10-10, RM-10-11, and RM-10-12). These ^{10}Be sampling locations are immediately inboard of the aforementioned coring locations, with the closest core sites being RM-10-1A, RM-10-1C, RM-10-1D, RM-12-4A, RM-12-4B, RM-12-5, and RM-10-3A. All ^{10}Be sample locations are outboard of core sites RM-12-1, RM-12-2A, RM-13-2B, and RM-13-3, as well as the earliest core sites K1 and K2 that were previously reported by Walker and Lowe (1977, 1979).

We sampled boulders that are well-embedded in geomorphologically stable positions at the crests of moraine ridges (Fig. 5). We avoided boulders located in sites that may have been disturbed by non-glacial post-depositional surface processes. Sampled surfaces were typically from the tops of well-rounded granitoid boulders. Deeply pitted, exfoliating, and/or spalled surfaces were avoided. We targeted surfaces that retained patches of glacial polish, glacially polished mineral grains, and/or glacial striae, all of which indicate minimal surface weathering since the time of deposition. Samples were collected using the drill-and-blast technique (Kelly, 2003) along with hammer and chisel. For each boulder sampled, we measured clast dimensions (long axis, short axis, and sample location height above ground measured on four sides), strike and dip, topographic shielding (measured azimuth and elevation at every inflection point on the skyline), and GPS coordinates. All sampled boulders were described, drawn, and photographed from every side.

We determined sample elevations from the Shuttle Radar Topography Mission (SRTM) digital elevation model in Google Earth in combination with the local Ordnance Survey 1:25,000 scale topographic map sheet with a contour interval of 10 m (Ordnance Survey, 2015). We found that Google Earth-derived elevations align well with contours plotted in the topographic map. All reported elevations are therefore derived from Google Earth and should be considered accurate to within ± 5 m (based on topographic map contours).

4.2. Laboratory methods

Following field collection, samples were shipped to the Lamont-Doherty Earth Observatory (LDEO) Cosmogenic Nuclide Laboratory for mineral separation and beryllium extraction using standard protocols. Mass-weighted sample thicknesses were measured using digital calipers. Samples were subsequently crushed, pulverized, and sieved to a grain-size range of 125–710 μm. These sample fractions were then subjected to boiling in concentrated H_3PO_4 and NaOH solutions. Some samples were further treated with froth-floatation mineral-separation techniques to separate feldspar. All samples were treated to successive etches in 2% HF/2% HNO_3 and 5% HF/5% HNO_3 solutions until only pure quartz remained. Pure quartz fractions were then weighed, spiked with ~180 μg of LDEO low-^{10}Be-background Be carrier, and then dissolved in concentrated (49%) HF. We used LDEO carrier 5 (initial ^{9}Be concentration = 1024 ± 10 ppm, based on multiple measurements). To correct for the increase in concentration of the carrier over time due to evaporation, the weight of the carrier bottle was recorded before and after each use. We calculated the percent change in weight and multiplied by the last corrected carrier concentration. This percent of concentration was added to the previous concentration to determine the evaporation-corrected concentration. Mass lost between uses of the

Table 3
Procedural blank ^{10}Be data.

Blank no.	CAMS laboratory no.	Sample ID	Corresponding samples	Carrier Added (g)	Carrier conc. (ppm)[a]	$^{10}Be/^{9}Be$ ± 1σ (10^{-16})[b]	N_{10Be} ± 1σ (10^3 atoms)[c]	^{9}Be current (μA)[d]	AMS Std[e]
1	BE34635	Blank_1_2012Dec07	RM-10-02, 03	0.1810	1030	1.057 ± 1.89	1.32 ± 2.35	16.0 (70%)	07KNSTD
2	BE34642	Blank_2_2012Dec21	RM-10-02, 03	0.1811	1030	3.437 ± 1.22	4.29 ± 1.52	18.9 (82%)	07KNSTD
3	BE35520	Blank_1_2013April15	RM-10-01	0.1833	1032	5.777 ± 1.10	7.30 ± 1.39	23.5 (88%)	07KNSTD
4	BE35522	Blank_2_2013April15	RM-10-01	0.1825	1032	9.516 ± 1.96	11.97 ± 2.47	20.7 (77%)	07KNSTD
5	BE38214	BLK1-2014Nov07	RM-10-06	0.1819	1036	0.450 ± 0.67	0.57 ± 0.84	25.6 (105%)	07KNSTD
6	BE38227	BLK2-2014Nov07	RM-10-06	0.1812	1036	2.343 ± 1.94	2.94 ± 2.43	24.8 (101%)	07KNSTD
7	BE38790	BLK2-2015Mar12	RM-10-10, 11	0.1814	1037	3.885 ± 1.05	4.88 ± 1.32	29.1 (107%)	07KNSTD
8	BE40326	BLK1-2015Dec10	RM-10-05, 09, 12	0.1835	1045	2.078 ± 1.06	2.66 ± 1.35	16.9 (64%)	07KNSTD
9	BE40548	BLK1-2016Jan11	RM-10-04, 07, 08	0.1835	1046	4.061 ± 1.32	5.21 ± 1.69	23.5 (98%)	07KNSTD

[a] Carrier concentrations have been corrected for evaporation.
[b] Boron-corrected $^{10}Be/^{9}Be$.
[c] Total ^{10}Be (in atoms) determined from each procedural blank.
[d] $^{9}Be^{+3}$ measured after the accelerator. Reported currents are those measured during the first run of each sample. In parentheses is the ratio, given in percent, of each sample current compared with the average of all measured first-run AMS standard currents.
[e] AMS standards to which respective ratios and concentrations are referenced. Reported $^{10}Be/^{9}Be$ ratio for 07KNSTD is 2.85×10^{-12}.

carrier solution was typically only a few milligrams, amounting to only a few 100ths of a percent, but this amounted to an increase in concentration of approximately 2% over 5 years. The rate of evaporation increases as the volume of solution remaining in the bottle decreases, and therefore the increase in concentration with time is not linear. The LDEO Carrier 5 ^{9}Be concentration was corrected for evaporation each time carrier was added to samples (see Tables 2 and 3 for corrected carrier concentrations).

After dissolution, beryllium was then separated from other common ions using ion-chromatography techniques based on Kohl and Nishiizumi (1992) and following the procedures from the University of Washington and Lamont-Doherty Earth Observatory laboratories, available online at: http://depts.washington.edu/cosmolab/chem.shtml and http://www.ldeo.columbia.edu/tcn. Each resulting BeO sample was combined with Nb powder, packed into stainless steel targets, and submitted to the Lawrence-Livermore National Laboratory Center for Accelerator Mass Spectrometry (LLNL CAMS) for $^{10}Be/^{9}Be$ measurement. Sample $^{10}Be/^{9}Be$ ratios were measured relative to the 07KNSTD3110 standard ($^{10}Be/^{9}Be = 2.85 \times 10^{-12}$; Nishiizumi et al., 2007), and corrected for boron contamination and machine backgrounds (each correction was typically < 1%).

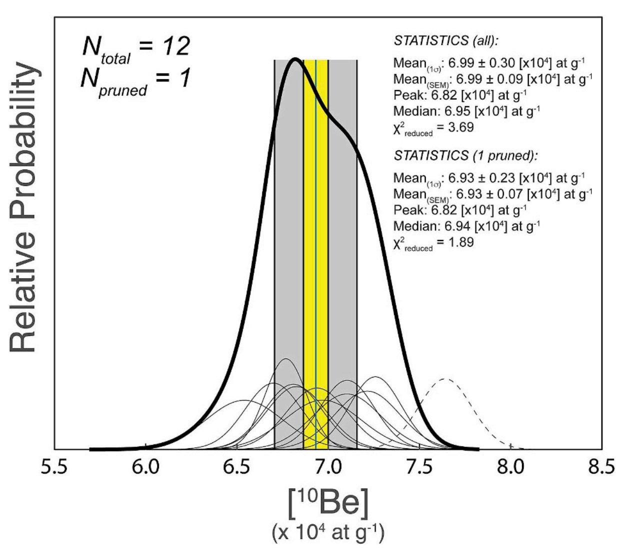

Fig. 6. Camel plot of measured ^{10}Be concentrations from the Rannoch Moor boulders. Concentrations have been corrected for thickness and topographic shielding, but not for differences in sample elevations. Thin, solid curves are Gaussian approximations of individual ^{10}Be analyses (given in Table 2). The thick solid curve represents the summed probability of the distribution. Thin, dashed line represents an anomalously high ^{10}Be concentration that is considered an outlier and excluded from further consideration. Gray vertical band represents the 1σ uncertainty of the distribution. Yellow vertical band represents the standard error of the mean. The vertical blue line denotes the arithmetic mean value of the distribution. Statistics are inset.

We determined ^{10}Be concentrations for 12 samples from the Rannoch Moor moraines. Samples were processed in six laboratory batches and measured in six CAMS runs spread over the course of five years (C.E. 2012–2016). To evaluate ^{10}Be contamination during laboratory procedures, we measured nine procedural laboratory blanks. The blanks afford ^{10}Be values that range between 570 and 11,970 ^{10}Be atoms per blank and yield an arithmetic mean of 4570 ± 3460 atoms (± 1σ). Blank concentrations correspond to < 1% of the total number of ^{10}Be atoms measured in our samples in the range of 1,000,000 atoms ^{10}Be. Reported ^{10}Be concentration uncertainties (Table 2) include the reported analytical uncertainty (1σ) propagated with uncertainties related to machine background, procedural blank, and boron corrections. Uncertainties related to background, blank, and boron corrections are each < 1%. Reported ^{10}Be concentration uncertainties are ~2% (1σ). Uncertainties related to ^{9}Be carrier concentration (~1%) were treated as systematic errors and incorporated into uncertainties calculated for the data set as a whole (and also propagated with production-rate uncertainties).

4.3. Production-rate calculation

Maximum- and minimum-limiting production rate values were calculated by comparing ^{10}Be concentrations measured in morainal boulders at Rannoch Moor with minimum- and maximum-limiting calendar-year-converted ^{14}C age constraints, respectively. The midpoint production-rate value was determined by comparing ^{10}Be concentrations with the age corresponding to the midpoint of the bracketing limiting ages (and uncertainty corresponding to the range of bracketing ages). Topographic shielding correction factors were calculated using the University of Washington (UW) online calculators available at: https://hess.ess.washington.edu.

We assume that erosion has been negligible (at least for the sampled surfaces) since the boulders were deposited, based on field observations of glacially polished surfaces/mineral grains present on sampled boulders. Likewise, winter snow cover is generally ephemeral at the elevations of the boulders sampled, and the open landscape of Rannoch Moor is susceptible to strong winds that would keep the boulders largely free of snow. We also note that any effects of erosion or snow cover would not necessarily be consistent from sample to sample and would

Table 4
Maximum-limiting, minimum-limiting, and midpoint ^{10}Be production rates determined from the Rannoch Moor moraines ('P_{RM}'), calculated with Version 3 of the UW online calculator using accepted scaling protocols. Recommended (i.e., midpoint) reference SLHL production-rate values/correction factors are given in bold. χ^2 values are given for 10 degrees of freedom (d.o.f). Expected χ^2 for 10 d.o.f. (evaluated at 95% confidence) = 18.31. 'St' and 'Lm' values are SLHL reference production rates, reported in units of [at g^{-1} yr^{-1}]. As described in text, LSDn results are presented as non-dimensional correction factors (applicable to the output production rates from the Lifton et al. (2014) model).

Scaling method	P_{RM} MAX	χ^2	P_{RM} MIN	χ^2	**P_{RM} MID**	χ^2
St	< 3.95 ± 0.11 (2.9%)	11.30	> 3.88 ± 0.11 (2.9%)	11.35	**3.91 ± 0.11 (2.9%)**	11.07
Lm	< 3.95 ± 0.11 (2.9%)	11.30	> 3.89 ± 0.11 (2.9%)	11.35	**3.92 ± 0.11 (2.9%)**	11.07
LSDn	< 0.787 ± 0.023 (2.9%)	11.38	> 0.773 ± 0.022 (2.9%)	11.42	**0.780 ± 0.022 (2.9%)**	11.14

likely increase the scatter among the ^{10}Be concentrations. Thus, we take the tight agreement among the ^{10}Be concentrations determined from the Rannoch Moor boulders (reported below) to indicate negligible impacts of erosion or snow cover on this dataset. Therefore, consistent with previous production-rate calibration efforts (e.g., Balco et al., 2009; Kaplan et al., 2011; Kelly et al., 2015; Putnam et al., 2010b; Young et al., 2013), the production-rate and exposure-age calculations reported below do not include corrections for erosion or snow cover.

Following previous studies (Balco et al., 2009; Kaplan et al., 2011; Putnam et al., 2010b; Young et al., 2013), we do not apply any correction for uplift in our production-rate or exposure-age calculations. Although there has been a viscoelastic response of the Earth's lithosphere to deglaciation in this region, the signature of post-glacial isostatic adjustment in central Scotland has been relatively minor compared to other production-rate calibration sites targeting deglaciated landscapes (e.g., Balco et al., 2009; Young et al., 2013). For example, the central Scottish Highlands have experienced only ~10 m or so of total vertical displacement with respect to modern sea level over the period of exposure and have been uplifting ~1 mm yr^{-1} over the past 1000 yrs or so (Lambeck, 1991; Stockamp et al., 2016)]. In addition, it is unclear how changes in air pressure related to deglaciation and eustatic sea-level rise may have counteracted the effects of uplift on production rates (Young et al., 2013). For these reasons we chose not to subject production-rate calculations to an uplift correction.

All production-rate determinations were calculated using Version 3 of the online UW cosmogenic calculators (https://hess.ess.washington.edu). This version of the calculator is broadly similar to earlier versions employed in previous production-rate calibration studies (e.g., Balco et al., 2009; Balco et al., 2008; Kaplan et al., 2011; Kelly et al., 2015; Putnam et al., 2010b; Young et al., 2013), but includes a few updates. Arguably the most important update to Version 3 of the UW calculator is the implementation of a revised (and simplified) calculation for muon production (Balco, 2017; Braucher et al., 2013). This muon production model replaces the Heisinger et al. (2002a; 2002b) protocols used in previous versions of the calculator, which were based on laboratory irradiation experiments. The Balco et al. (2017) model predicts a SLHL muon production rate of 0.0735 at g^{-1} yr^{-1}, which, for example, accounts for only 1.8% of total production if the SLHL neutron spallation rate at a rock surface is 4.0 at g^{-1} yr^{-1} (and 1.9 % if the reference SLHL neutron spallation rate is 3.9 at g^{-1} yr^{-1}). To determine the SLHL 'reference' production rate for neutron spallation only, the UW production-rate calculator first subtracts the muonogenic component, scaled for latitude and altitude, from the total measured ^{10}Be production. The remaining (~98%) of the ^{10}Be is referenced to SLHL, or else evaluated against a modeled local reference production-rate value, using one of three scaling models (described below) to determine the neutron-produced component of the total ^{10}Be inventory.

It is important to note that the Balco (2017) protocol for determining ^{10}Be production by muons predicts a lower muon production rate than the previously implemented Heisinger et al. (2002a; 2002b) framework. As such, all reported values for neutron spallation production rates calculated with Version 3 of the UW online production-rate calculator are systematically ~2% higher than previously reported values. However, because muon production accounts for such a small percentage of surface production, this procedural change has virtually no impact on surface-exposure chronologies calculated using the same production-rate calibration data sets but with previous versions of the UW calculator (although studies of erosion rates or burial may be affected).

Version 3 of the UW calculator references an atmosphere model based on the ERA-40 Reanalysis data set (Uppala et al., 2005) for site-specific air-pressure information, and includes the Lifton et al. (2014) scaling model ('LSDn') in addition to the Lal (1991)/Stone (2000) ('St') and Lal/Stone time-dependent ('Lm') models used in previous versions of the calculator. Full documentation of Version 3 of the UW calculators is available online at: https://sites.google.com/a/bgc.org/v3docs/.

In order to facilitate comparison of production-rate calibration sites at different locations, we used Version 3 of the UW online calculator to determine production rates referenced to SLHL using the 'St' and 'Lm' scaling models. Because the LSDn model produces site-specific production rates (in atoms g^{-1} yr^{-1}) as opposed to non-dimensional scaling factors that apply to reference SLHL production rates (such as with the St and Lm scaling models), and because the reference production rates used in the LSDn model differ from those of the other models (related to how the LSDn model accounts for solar/magnetic variability), the UW online calculator provides a non-dimensional correction factor that represents the offset between the independently calibration production rate and that determined by the LSDn model (G. Balco, personal communication, 10 September 2017). Therefore, to maintain consistency with the reporting procedures of the UW online calculators, we also report non-dimensional correction factors for the LSDn production-rate scaling model rather than SLHL reference production-rate values, as output by Version 3 of the UW online calculator.

Production-rate uncertainties attending the Rannoch Moor results are calculated by the 'total scatter' method in Version 3 of the UW online calculator. This method accounts for the standard deviation of the individual measurements, as well as the χ^2 of the population with respect to a best-estimate value. We also incorporate a 1% carrier-concentration uncertainty into the overall Rannoch Moor production-rate uncertainty estimate (i.e., propagated in quadrature with the total-scatter uncertainty).

To maintain consistency with the production-rate calculations employed for the Rannoch Moor data set, we re-calculated production rates and attendant uncertainties from previously published calibration data sets using these same methods. SLHL production rates and correction factors for previously published calibration data sets have also been calculated using Version 3 of the UW online calculator with the data tables supplied by the ICE-D production-rate calibration database (http://calibration.ice-d.org). For single-site calibration sites, we employed the 'total scatter' method for determining uncertainties. For production-rate calculations involving previously published calibration data sets based on multiple sites, uncertainties were determined using the 'site-to-site scatter' calculation in the online calculator, which is derived from the standard deviations of each calibration site and the corresponding χ^2 for the best-estimate value of the combined data sets (see the documentation for Version 3 of the UW online calculators for a

Table 5a
Maximum-limiting, minimum-limiting, and midpoint ^{10}Be production rates determined from the Rannoch Moor moraines ('P_{RM}'), using accepted scaling protocols, compared to other SLHL reference production rates mentioned in text. As described in text, LSDn results are presented as non-dimensional correction factors (applicable to the output production rates from the Lifton et al. (2014) model. 'St' and 'Lm' values are SLHL reference production rates, reported in units of [at g^{-1} yr^{-1}]. 'GLOBAL' refers to the primary global calibration data set of Borchers et al. (2016). 'BB' refers to the Baffin Bay calibration sites of Young et al. (2013). 'SWISS' refers to the data set of Claude et al. (2014) from the Chironico landslide deposit in southern Switzerland. 'NENA' refers to the northeastern North American calibration data set of Balco et al. (2009). 'PERU1' refers to the calibration data set of Kelly et al. (2015) from the tropical Peruvian Andes. 'PERU2' refers to the calibration data set of Martin et al. (2015) from the tropical Peruvian Andes. 'NZ' refers to the Macaulay valley calibration site in the Southern Alps of New Zealand of Putnam et al. (2010). 'PAT' refers to the Patagonian calibration sites of Kaplan et al. (2011). Uncertainties for single-site calibration data sets were calculated by 'total scatter' in Version 3 of the UW online calculator (SWISS, PERU1, PERU2, NZ). Uncertainties for calibration data sets containing multiple sites were calculated by site-to-site' scatter (GLOBAL, BB, NENA, PAT). With the exception of the GLOBAL data set, all calibrations are underpinned by absolute, site-specific ^{14}C or U/−Th dating control. Recommended (i.e., midpoint) reference production-rate values/correction factors are given in bold.

Scaling method	P_{GLOBAL}	P_{BB}	P_{SWISS}	P_{NENA}	P_{PERU1}	P_{PERU2}	P_{NZ}	P_{PAT}	P_{RM} MAX	P_{RM} MIN	**P_{RM} MID**
St	4.13 ± 0.16 (3.8%)	4.03 ± 0.015 (0.4%)	3.98 ± 0.13 (3.1%)	4.04 ± 0.26 (6.3%)	3.98 ± 0.21 (5.2%)	4.04 ± 0.26 (6.3%)	3.92 ± 0.06 (1.6%)	3.89 ± 0.07 (1.7%)	< 3.95 ± 0.11 (2.9%)	> 3.88 ± 0.11 (2.9%)	**3.91 ± 0.11 (2.9%)**
Lm	4.22 ± 0.11 (2.7%)	4.03 ± 0.015 (0.4%)	4.014 ± 0.13 (3.1%)	4.04 ± 0.25 (6.2%)	4.36 ± 0.23 (5.4%)	4.18 ± 0.26 (6.3%)	4.01 ± 0.06 (1.6%)	4.01 ± 0.06 (1.5%)	< 3.95 ± 0.11 (2.9%)	> 3.89 ± 0.11 (2.9%)	**3.92 ± 0.11 (2.9%)**
LSDn	0.846 ± 0.016 (1.9%)	0.776 ± 0.008 (1.1%)	0.836 ± 0.027 (3.2%)	0.856 ± 0.071 (8.3%)	0.835 ± 0.044 (5.3%)	0.852 ± 0.053 (6.3%)	0.847 ± 0.013 (1.6%)	0.835 ± 0.011 (1.4%)	< 0.787 ± 0.023 (2.9%)	> 0.773 ± 0.022 (2.9%)	**0.780 ± 0.022 (2.9%)**

complete explanation of uncertainty determinations: https://sites.google.com/a/bgc.org/v3docs/home/2-input-and-output).

We note that the site-to-site averaging method employed in the UW online production-rate calculator differs slightly from the method employed in Borchers et al. (2016). Whereas the calculation of Borchers et al. (2016) weights sites by the precision of independently known landform ages, the averaging method employed in Version 3 of the UW online production-rate calculator weights all sites equally (Balco, personal communication, 25 June 2018). Thus, the calibration results reported here for the Borchers et al. (2016) data set may differ slightly from those reported in the original paper. In addition, we note that we removed a small number of apparent outlier measurements (determined from Version 3 of the UW online calculator, based on $\chi 2$ statistics) from three data sets before calculating production rates: One anomalously low-concentration measurement from the data set of Kaplan et al. (2011; sample EQ-08-04), two anomalously high-concentration samples from the dataset of Martin et al. (2015; samples AZA-30 and AZA-32), and one anomalously high-concentration sample and one anomalously low-concentration sample from the data set of Claude et al. (2014; samples CHI-11 and CHI-10). Finally, to maintain consistency with the approach outlined above, we did not include any corrections for erosion, snow cover, or uplift in our analysis of these previously published data sets.

5. Results

5.1. ^{10}Be data

Measured ^{10}Be concentrations exhibit tight internal consistency and form an approximately normal distribution when corrected for thickness and topographic shielding (Fig. 6). Uncorrected concentrations range from 6.66 ± 0.22 to 7.70 ± 0.15 [x10^4] at g^{-1} (Table 2). Only one measurement (RM-10-01; 7.70 ± 0.15 [x10^4] at g^{-1}) has a distinguishably different (i.e., higher) concentration from the rest of the population. If treated as a surface-exposure age (as a means of normalizing the measurements for the effects of pressure elevation, sample thickness, topographic shielding, etc.), the corresponding age is distinguishably older than the rest of the data set and is flagged as an outlier by Version 3 of the UW online exposure age calculator (Balco et al., 2008; and subsequent updates). Therefore, we consider this measurement to be an outlier and exclude it from further assessment of production rates or exposure ages. The remaining eleven samples yield uncorrected concentrations ranging from 6.66 ± 0.22 to 7.35 ± 0.18 [x10^4] at g^{-1}, with an arithmetic mean of 7.01 ± 0.23 [x10^4] at g^{-1} ($N = 11$; uncorrected for thickness or topographic shielding; uncertainty is 1σ propagated in quadrature with a conservative 1% systematic uncertainty related to carrier concentration). The arithmetic mean of the thickness- and shielding-corrected concentrations is 6.93 ± 0.24 [x10^4] at g^{-1} and yields a reduced-χ^2 value of 1.89 (Fig. 6). Although this latter arithmetic mean value accounts for sample thickness and topographic shielding, the constituent concentrations are not corrected for minor differences in sample elevation from 313 to 327 m a.s.l. The striking internal consistency (and low-χ^2 value) indicate that the remaining scatter in the ^{10}Be concentrations of the individual samples can be explained by analytical uncertainties (Balco and Schaefer, 2006; Bevington and Robinson, 1992).

5.2. ^{10}Be production rates

Dividing the arithmetic mean of the measured ^{10}Be concentrations of 6.92 ± 0.24 [x10^4] at g^{-1} yr^{-1} by the midpoint age of 12,590 ± 140 yrs for the Rannoch Moor moraine belt yields the total local ^{10}Be production rate of 5.50 ± 0.18 at g^{-1} yr^{-1} (this value is not corrected for elevation differences among sampled surfaces). This result was then transformed to SLHL values using the scaling models incorporated into Version 3 of the UW online production-rate calculator

Table 5b
Comparison of production rates given in Table 5a relative to the Rannoch Moor production rates from this study.

Scaling	P_{RM}/P_{GLOBAL}	P_{RM}/P_{BB}	P_{RM}/P_{SWISS}	P_{RM}/P_{NENA}	P_{RM}/P_{PERU1}	P_{RM}/P_{PERU2}	P_{RM}/P_{NZ}	P_{RM}/P_{PAT}
method								
St	0.95	0.97	0.98	0.97	0.98	0.97	1.00	1.01
Lm	0.93	0.97	0.98	0.97	0.90	0.94	0.98	0.98
LSDn	0.92	1.01	0.93	0.91	0.93	0.92	0.92	0.93

and removed of the muon-produced ^{10}Be component. All SLHL production-rate results reported here are therefore for neutron spallation only and summarized in Table 4. The non-time-dependent 'St' scaling model yields SLHL reference maximum, minimum, and midpoint ^{10}Be production rates of $< 3.95 \pm 0.11$ at g^{-1} yr^{-1}, $> 3.88 \pm 0.11$ at g^{-1} yr^{-1}, and 3.91 ± 0.11 at g^{-1} yr^{-1}, respectively. The time-dependent 'Lm' scaling model yields SLHL reference maximum, minimum, and midpoint ^{10}Be production rates of $< 3.95 \pm 0.11$ at g^{-1} yr^{-1}, $> 3.89 \pm 0.11$ at g^{-1} yr^{-1}, and 3.92 ± 0.11 at g^{-1} yr^{-1}, respectively. Finally, the time-dependent 'LSDn' scaling model yields maximum, minimum, and midpoint ^{10}Be production-rate correction factors of $< 0.787 \pm 0.023$ at g^{-1} yr^{-1}, $> 0.773 \pm 0.022$ at g^{-1} yr^{-1}, and 0.780 ± 0.022 at g^{-1} yr^{-1}, respectively. All production-rate calculations yield low χ^2 values between 11.07 and 11.42 relative to an expected theoretical value for a Gaussian distribution of the same population size.

Input data sets for use with the UW online exposure calculators are provided online in the Mendeley open-access data repository (see Data Availability section, below).

6. Discussion

Here we discuss the calibration data set presented in this study within the context of: (i) distal calibration data sets based on landforms with direct independent age control, (ii) previously published calibration data sets from indirectly dated landforms in the Scottish Highlands, and (iii) previously published ^{10}Be data sets from the Rannoch Moor region.

6.1. Comparison to distal ^{10}Be production-rate calibration data sets

Here, we evaluate how the Rannoch Moor calibration data set aligns with other comparable calibration efforts from around the world. Tables 5 and 6 compare SLHL production rates (for 'St' and 'Lm' scaling models) and production-rate correction factors (for 'LSDn' scaling) reported in this study for Rannoch Moor with previously published production-rate calibration sites from different latitudes and altitudes with absolute independent age constraints. Fig. 7 compares the results of all calibration data sets for the three scaling models and normalized to Rannoch Moor values. All SLHL production-rate values (and LSDn correction factors) have been calculated using Version 3 of the UW online production-rate calculator. Specifically, we compare the Rannoch Moor data set with those from northeastern North America (Balco et al., 2009), the Canadian Arctic (i.e., Baffin Bay; Young et al., 2013), Switzerland (Claude et al., 2014), Peru (Kelly et al., 2015; Martin et al., 2015), New Zealand (Putnam et al., 2010b), and southern South America (Kaplan et al., 2011). In addition, for reference, we consider production rates from the primary global calibration data set of Borchers et al. (2016; also the default calibration data set in Version 3 of the UW online calculator) which includes some ^{10}Be measurements from landforms that are not directly dated (see section 2.0, above).

In general, when scaled using currently accepted protocols, the results reported here for the Rannoch Moor ^{10}Be calibration site agree well with results from calibration sites with comparable independent age control, mentioned above (Tables 5 and 6; Fig. 7). All scaling models produce reasonably good agreement. The best overall empirical agreement among these disparate sites is achieved with the non-time-dependent 'St' scaling protocol. By this scaling method, all of the regional calibrations yield production-rate values that agree with the Rannoch Moor value, within respective uncertainties. The best empirical agreement is between the Rannoch Moor and New Zealand values. The time-dependent 'Lm' scaling model yields general agreement among Rannoch Moor and other middle and high-latitude sites, but with less coherence among the Rannoch Moor and tropical/high-altitude (Peruvian) data sets. The 'LSDn' scaling model produces the least amount of convergence among production-rate correction factors determined from Rannoch Moor and other comparable calibration data sets. Whereas results from sites in the Southern Hemisphere, tropics, and Switzerland tend to show close agreement among one another, those sites exhibit little to no overlap with the result from Rannoch Moor (considering respective uncertainties). On the other hand, the result from Baffin Bay shows close agreement with that from Rannoch Moor when calculated using the LSDn scaling model.

The Rannoch Moor calibration data set presented here yields SLHL production-rate values for 'St' and 'Lm' scaling models, and a production-rate correction factor for the 'LSDn' model, that are 5%, 7%, and 8% lower, respectively, than the globally averaged values determined from the primary calibration data set of Borchers et al. (2016). Using our ^{10}Be data from Rannoch Moor, the primary calibration data set of Borchers et al. (2016) produces surface-exposure ages that are 2–5% too young with respect to minimum-limiting ^{14}C-age constraints (depending on the scaling model used).

We note that the production-rate calibration data set presented here eliminates the unexplained discordance among production-rate calibrations from Scotland and elsewhere on Earth, as identified by Phillips et al. (2016). Whereas this discrepancy was previously attributed to problems relating to scaling models, perhaps involving anomalous changes in atmospheric pressure related to deglaciation, we hypothesize that the scaling models do a reasonably good job of reconciling calibration data that are based solely on landforms with direct radiometric chronological control.

6.2. Comparison with other Scottish calibration data sets

Table 6 provides SLHL production rates and correction factors determined from the Coire Mhic Fearchair, Maol Chean Dearg, Corie nan Arr, and Glen Roy data sets, for comparison to the results presented in this study from Rannoch Moor. Overall, these previously published calibration data sets yield SLHL production-rate estimates/correction factors that are ~6–8% higher (depending on choice of scaling model, with erosion rates set to zero) than our Rannoch Moor calibration data set, based on the midpoint age assignment, and ~4–7% higher than the maximum-limiting production rate determined from Rannoch Moor (based on minimum-limiting ^{14}C data for plant colonization). See Table 6b for comparison of production-rate ratios. Inclusion of erosion rates proposed in the original publications further increases the offsets by ~1%. The discrepancy in production-rate estimates translates to surface-exposure ages that are at least 4–7% too young to be consistent with the independent ^{14}C chronology at Rannoch Moor. We consider that this observed disagreement between ^{14}C and ^{10}Be chronologies can be explained by calibration landforms having older ages than initially assumed in previous calibration studies (Ballantyne and Stone, 2012;

Table 6a
Production rates determined from previously published Scottish Highland sites mentioned in text, calculated using Version 3 of the UW online calculator with accepted scaling protocols. LSDn results are presented as non-dimensional correction factors (applicable to the output production rates from the Lifton et al. (2014) model). 'St' and 'Lm' values are SLHL reference production rates, reported in units of [at g^{-1} yr^{-1}]. The maximum, minimum, and midpoint ^{10}Be production rates from this study are provided for reference. Recommended (i.e., midpoint) reference production-rate values/correction factors are given in bold. We removed one anomalously high-concentration sample from the Coire nan Arr data set, and one low-concentration sample from the Glen Roy data set. All calculations were conducted assuming zero erosion.

Scaling method	Coire nan Arr	χ^2	Maol Chean Dearg	χ^2	Coire Mhic Fearchair	χ^2	Glen Roy	χ^2	P_{RM} MAX	χ^2	P_{RM} MIN	χ^2	**P_{RM} MID**	χ^2
St	4.21 ± 0.11 (2.6%)	14.96	4.17 ± 0.05 (1.2%)	0.77	4.23 ± 0.22 (5.1%)	4.85	4.24 ± 0.042 (1.0%)	0.07	< 3.95 ± 0.11 (2.7%)	11.30	> 3.88 ± 0.11 (2.7%)	11.35	**3.91 ± 0.11 (2.7%)**	11.07
Lm	4.21 ± 0.11 (2.6%)	14.95	4.18 ± 0.05 (1.2%)	0.77	4.24 ± 0.22 (5.2%)	4.87	4.24 ± 0.042 (1.0%)	0.07	< 3.95 ± 0.11 (2.7%)	11.30	> 3.89 ± 0.11 (2.7%)	11.35	**3.92 ± 0.11 (2.7%)**	11.07
LSDn	0.829 ± 0.022 (2.6%)	14.84	0.831 ± 0.01 (1.2%)	0.77	0.844 ± 0.044 (5.2%)	4.97	0.845 ± 0.008 (1.0%)	0.07	< 0.787 ± 0.021 (2.7%)	11.38	> 0.773 ± 0.021 (2.7%)	11.42	**0.780 ± 0.021 (2.7%)**	11.14

Borchers et al., 2016).

An additional observation is that the Coire Mhic Fearchair, Maol Chean Dearg, and Corie nan Arr data sets (Ballantyne and Stone, 2012; Borchers et al., 2016) yield surface-exposure chronologies that are indistinguishable from that at Rannoch Moor when all ages are calculated using a common production-rate calibration data set. For example, when using the Rannoch Moor production-rate calibration data set (this study) and 'St' scaling, we obtain arithmetic mean ages [± 1σ] of 12,710 ± 650 yrs, 12,510 ± 150 yrs, and 12,620 ± 330 yrs for the Coire Mhic Fearchair, Maol Chean Dearg, Corie nan Arr data sets, respectively. Compared to the mean ^{10}Be surface-exposure value obtained for Rannoch Moor of 12,650 ± 340 yrs (using the same calculation method), all data sets are statistically indistinguishable within respective uncertainties, with arithmetic mean values deviating by only 200 yrs or less. Choice of a different scaling model does not alter this result. Therefore, the hypothetical case can be made that the erratic boulders sampled from the corrie glacier systems described in Ballantyne and Stone (2012) were all exposed, and hence deglaciated, at the same time as Rannoch Moor, within respective uncertainties.

When recalculating the Glen Roy ^{10}Be chronology (Small and Fabel, 2015) using the Rannoch Moor production-rate calibration data set presented here, surface-exposure ages from the ~325-m shoreline at Glen Roy (one sample with a 50-cm peat cover was omitted, consistent with treatment of this data set in the ICE-D database) afford an arithmetic mean value of 13,060 ± 130 yrs [± 1σ]. This landform age is consistent with the range of ^{14}C ages obtained for the WHIF moraines and tills reported in Bromley et al. (2018).

6.3. Comparison with other ^{10}Be data from Rannoch Moor

Two previous studies provided ^{10}Be data from the Rannoch Moor region and afford an opportunity for interlaboratory and inter-AMS comparison with [^{10}Be] data presented in this study. The first ^{10}Be data from this area, published by Golledge et al. (2007), were from erratic boulders mantling the nearby summit ridge of Beinn Inverveigh (~580–620 m a.s.l.), located approximately 10-km SSW of Rannoch Moor. Beinn Inverveigh has been variably mapped as having stood above the full-bodied late-glacial WHIF (Thorp, 1984, 1986), or as having been fully ice-covered by the WHIF (Golledge, 2007). The chronology of erratic boulders was therefore used to determine the thickness of the WHIF at its full late-glacial configuration (Golledge, 2007, 2010; Golledge et al., 2007). In any case, these higher-elevation boulders would have been exposed to the cosmic-ray flux prior to the boulders rooted in the Rannoch Moor moraine belt, which were exposed during the final phase of WHIF disintegration. Thus, this morphostratigraphic age difference should be reflected in the measured [^{10}Be] inventory of these data sets. Calculation of the Golledge et al. (2007) ^{10}Be surface-exposure data set using the Rannoch Moor calibration data set yields ages of 13,270 ± 880 yrs (BI 1), 14,280 ± 620 yrs (BI 2), 14,760 ± 800 yrs (BI 3), and 14,600 ± 1400 yrs (BI 4) documenting the height of the WHIF during late-glacial time (ages were corrected for AMS standardization and calculated using St scaling in Version 3 of the UW online calculator, for illustrative purposes, although all scaling models afford similar ages, given the proximity of the samples to the Rannoch Moor calibration site). These results are morphostratigraphically concordant with the ^{10}Be data presented here, and are also in agreement with the span of ^{14}C ages on WHIF tills and moraines marking advances toward full late-glacial limits between ~14,600 and 12,800 cal yrs ago (Bromley et al., 2018). Thus, the data set of Golledge et al. (2007) may serve to constrain the height of the full-bodied WHIF of late-glacial time.

In addition, Small and Fabel (2016b) presented a ^{10}Be dataset from boulders rooted in the same Rannoch Moor moraine belt targeted here, and in one case from the same boulder sampled by our team in C.E. 2010. Overall, the Small and Fabel (2016b) data set exhibits good internal consistency, with a tight cluster of four surface-exposure ages and

Table 6b
Comparison of published Scottish production rates (Table 6a) relative to the Rannoch Moor production rates from this study. Abbreviations: 'RM' is Rannoch Moor; 'CnA' is Coire nan Arr; 'MCD' is Maol Chean Dearg; 'CMF' is Coire Mhic Fearchair; 'GR' is Glen Roy.

Scaling	P_{RM}/P_{CnA}	P_{RM}/P_{MCD}	P_{RM}/P_{CMF}	P_{RM}/P_{GR}	P_{RM}/P_{CnA}	P_{RM}/P_{MCD}	P_{RM}/P_{CMF}	P_{RM}/P_{GR}
method	(P_{RM} midpoint)				(P_{RM} maximum limit)			
St	0.93	0.94	0.92	0.92	0.94	0.95	0.93	0.93
Lm	0.93	0.94	0.92	0.92	0.94	0.94	0.93	0.93
LSDn	0.94	0.94	0.92	0.92	0.95	0.95	0.93	0.94

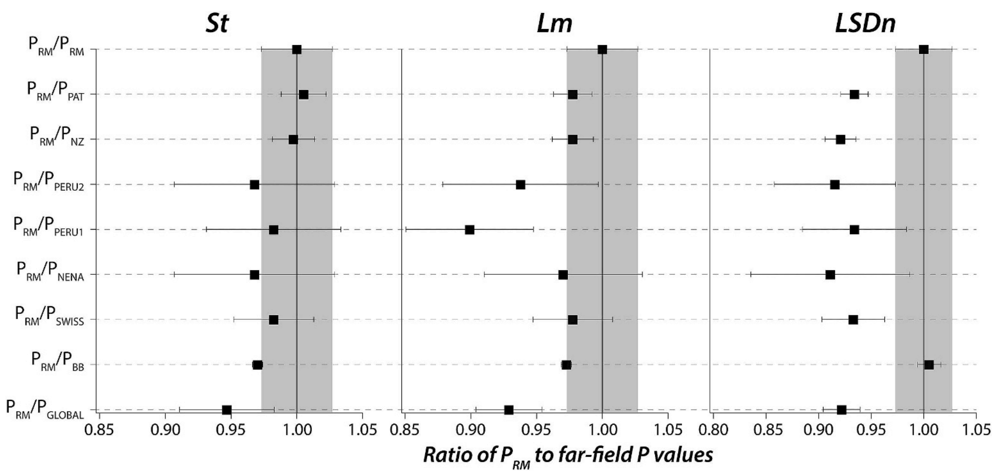

Fig. 7. Comparison of Rannoch Moor production rates and correction factors (P_{RM}) with a set of distal production-rate calibration data set for the 'St', 'Lm', and 'LSDn' scaling models. Values are presented as ratios and normalized to the Rannoch Moor value. The vertical gray bands represent the Rannoch Moor production-rate uncertainties. Abbreviations for selected calibration data sets are as follows: 'PAT' = Patagonia (Kaplan et al., 2011), 'NZ' = New Zealand (Putnam et al., 2010a), 'PERU1' = Peru (Kelly et al., 2015), 'PERU2' = Peru (Martin et al., 2015), 'NENA' = Northeast North America (Balco et al., 2009); 'SWISS' = Switzerland (Claude et al., 2014), 'BB' = Baffin Bay (Young et al., 2013), and 'GLOBAL' = the primary global calibration data set of Borchers et al. (2016).

two older samples rejected as outliers. On the basis of this data set, Small and Fabel (2016b) suggested that, regardless of which production-rate calibration data set is used, none is sufficient to produce a ^{10}Be chronology for their data set that is compatible with the minimum-limiting ^{14}C dates at Rannoch Moor. This apparent discordance led the authors to question the validity of the Rannoch Moor ^{14}C data set, which in turn triggered a comment and reply that discussed some of the underlying issues in greater detail (Bromley et al., 2016; Small and Fabel, 2016a).

We report the observation that the [^{10}Be] concentrations presented here are systematically higher than those reported by Small and Fabel (2016b). Comparison of the mean values of the [^{10}Be] distributions (pruned of outliers and corrected for thickness and shielding) yields an offset of 7.7%. The difference increases slightly to 7.9% when accounting for differences in sample elevation (this was achieved by calculating nominal exposure ages for the whole data set using the St scaling protocol and the Rannoch Moor production rate presented here; Fig. 8). A χ^2 test of the combined data sets (minus outliers) yields an overall χ^2 value of 49.96. When compared to the theoretical expected value of 23.68 for a Gaussian distribution of the same population size (evaluated at 95% confidence), this result indicates that the two data sets form distinct statistical populations. Furthermore, Small and Fabel (2016b) happened to acquire their sample RMOOR04 from the same boulder surface as our sample RM-10-08 (see Figs. 1 and 5; and Table 1 for boulder coordinates), thus permitting a true interlaboratory comparison. Small and Fabel (2016b) reported a [^{10}Be] for RMOOR04 of 6.65 ± 0.17 [x10^4] at g^{-1}. This value is 5.8% lower than that reported here from sample RM-10-08 for the same rock surface (7.06 ± 0.21 [x10^4] at g^{-1}; this study). When corrected for sample thickness, the difference is 5.5%. In either case, the magnitude of the offset exceeds the analytical uncertainties of each measurement. In light of this comparison, we consider that the source of the offset between the two data sets is somehow related to the ^{10}Be concentration data, and not due to sample selection.

At this time, the source of the offset between the Small and Fabel (2016b) data set and the data presented here is unclear. However, we can confirm that the ^{10}Be data in this study were generated in a manner that is internally consistent (i.e., same methods, same laboratory, same accelerator, and all relative to the same 07KNSTD AMS standard), and thus should be directly comparable with several other primary geological calibration data sets (e.g., Kaplan et al., 2011; Kelly et al., 2015; Putnam et al., 2010b; Young et al., 2013). This apparent offset in reported ^{10}Be measurements highlights the value of interlaboratory comparison (Jull et al., 2015). Therefore, to get to the bottom of the noted discrepancy in reported ^{10}Be measurements from Rannoch Moor, we are now coordinating a collaborative inter-laboratory comparison between LDEO/CAMS and the Scottish Universities Environmental Research Center (SUERC) AMS laboratories (D. Fabel, personal communication, 06 August 2018).

7. Conclusions

1) We present a geological ^{10}Be production-rate calibration based on the Rannoch Moor moraine belt of the central Scottish Highlands (56.63°N, 4.77°W; ~310–330 m a.s.l.).
2) The landforms targeted for production-rate calibration are bracketed by twenty-seven maximum- and twenty minimum-limiting ^{14}C ages. This ^{14}C chronology indicates that the Rannoch Moor moraines were formed no earlier than 12,700 ± 100 cal. yrs BP, and no later than 12,480 ± 110 cal yrs BP. On the basis of these bracketing ages, we assigned a midpoint age of 12,590 ± 140 cal yrs BP for when the Rannoch Moor moraines were constructed, and hence when the sampled boulders commenced their exposure to the cosmic-ray flux.
3) We measured ^{10}Be concentrations from the surfaces of twelve boulders rooted in the Rannoch Moor moraine belt. The samples yield an arithmetic mean ^{10}Be concentration (± 1σ) of 6.93 ± 0.23 [x10^4] at g^{-1} (N = 11) after pruning one anomalously high ^{10}Be concentration (RM-10-01; 7.70 ± 0.15 [x10^4] at g^{-1}). Together, the ^{14}C chronology and ^{10}Be measurements from Rannoch

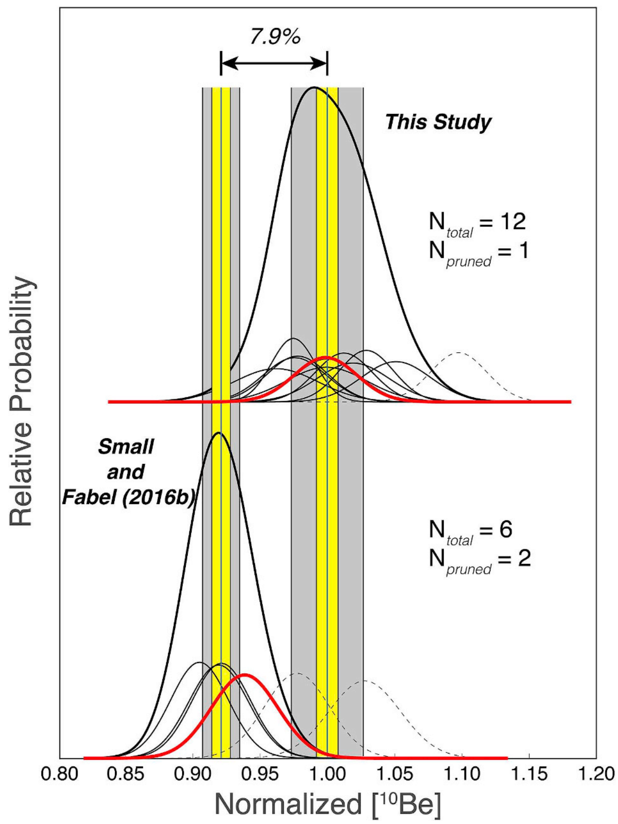

Fig. 8. Comparison of Rannoch Moor ^{10}Be data from this study (top) and from Small and Fabel (2016b) (bottom). ^{10}Be concentrations have been corrected for thickness and topographic shielding, scaled to SLHL (using the 'St' scaling model), and normalized to the arithmetic mean value of the data reported in this study. We note that the observed offset in ^{10}Be distributions is independent of choice of scaling model used to correct for differences in boulder-sample elevations. Thin black curves are Gaussian approximations of individual sample analyses. Thick black lines are summed probability curves for each distribution. Thin, dashed lines are Gaussian representations of samples with anomalously high concentrations (treated as outliers). Vertical gray bands represent 1σ uncertainties for each distribution. Yellow bands represent the standard error of the mean for each distribution. Vertical blue lines correspond to arithmetic means for each distribution. Bold red lines refer to the Gaussian representations of samples RM-10-08 (top) and RMOOR04 (bottom), which were each collected from the same boulder surface. Note that the overall distributions are offset by ~7.9%. RM-10-08 and RMOOR04, collected from the same rock surface, exhibit an offset of ~5.5%.

Moor moraine boulders yield a local site-specific total ^{10}Be production rate of 5.50 ± 0.18 at g^{-1} yr^{-1} (i.e., including production both by muons and neutrons).

4) We used the calibration data set from Rannoch Moor with Version 3 of the UW online production-rate calculator to determine reference SLHL production rates [for neutron spallation only; muon-produced ^{10}Be subtracted according to Balco (2017)] of 3.91 ± 0.11 and 3.92 ± 0.11 at g^{-1} yr^{-1} using the 'St' and 'Lm' scaling models, respectively, and a production-rate correction factor of 0.780 ± 0.022 at g^{-1} yr^{-1} using the 'LSDn' model. To facilitate comparison among production rates determined from elsewhere, we recalculated all far-field calibration data consistently using these methods.
5) The SLHL reference production rates presented here agree well with other widely distributed calibration data sets that are also based on landforms with direct and independent chronological control.
6) The resulting reference ^{10}Be production-rate values from Rannoch Moor are 5–8% lower than those determined using the primary global calibration data set presented in Borchers et al. (2016). In other words, applying the primary global ^{10}Be production-rate calibration would yield Rannoch Moor exposure ages that are 2–5% younger than, and hence do not agree with, the independent minimum-limiting ^{14}C chronology. The ^{10}Be production rates are also lower than the three previously published ^{10}Be production-rate values from Scotland. We consider the hypothesis that the primary global calibration data set is biased toward those earlier Scottish studies that are based on landforms that do not have direct chronological control, but are instead tuned to distal proxy records. The ^{10}Be production-rate data from Rannoch Moor, presented here, resolves these discrepancies by producing surface-exposure ages that accord with local ^{14}C chronologies.
7) Overall, the production-rate-calibration data set presented here can be used in conjunction with the UW online calculators for generating surface-exposure chronologies for the British Isles, and perhaps farther afield, that are compatible with independent ^{14}C chronologies.

Data Availability

The calibration data set related to this article can be found at the open-source online data repository hosted at Mendeley Data.

Acknowledgements

The authors wish to thank M.R. Kaplan, G.H. Denton, B.L. Hall, T.V. Lowell, J. Stone, C. Fenton, and many others for insightful discussions over the years. We are particularly grateful to G. Balco for sharing his knowledge and providing advice on the technical aspects of production-rate calculation. G. Balco's 'cosmognosis' blog has also been very helpful. D. Fabel and D. Small provided helpful discussion regarding ^{10}Be data from Rannoch Moor. M. Kelly and R. Braucher provided constructive comments that improved the paper. We acknowledge support from the Dan and Betty Churchill Exploration Fund and the Lamont-Doherty Earth Observatory (LDEO) Climate Center. A.E.P and G.R.M.B. each acknowledge support from the LDEO Postdoctoral Fellowship. A.E.P. acknowledges the Lenfest Foundation, the Comer Family Foundation, and the Quesada Family Fund. J.M.S. acknowledges support from the Lamont Climate Center. We thank R. Schwartz and J. Frisch for assistance in the laboratory, as well as D. Duerden, E. Watson, and H. Senn for their help during field work at Rannoch Moor. This is LDEO contribution number 8267.

References

Balco, G., 2011. Contributions and unrealized potential contributions of cosmogenic-nuclide exposure dating to glacier chronology, 1990-2010. Quat. Sci. Rev. 30, 3–27.
Balco, G., 2017. Production rate calculations for cosmic-ray-muon-produced ^{10}Be and ^{26}Al benchmarked against geological calibration data. Quat. Geochronol. 39, 150–173.
Balco, G., 2018. ICE-D: informal cosmogenic nuclide exposure-age database. Production-rate calibration data, accessed, October 2018. http://calibration.ice-d.org (Accessed October 2018).
Balco, G., Briner, J.P., Finkel, R., Rayburn, J.A., Ridge, J.C., Schaefer, J.M., 2009. Regional beryllium-10 production rate calibration for late-glacial northeastern North America. Quat. Geochronol. 4, 93–107.
Balco, G., Schaefer, J.M., 2006. Cosmogenic-nuclide and varve chronologies for the deglaciation of southern New England. Quat. Geochronol. 1, 15–28.
Balco, G., Stone, J.O., Lifton, N.A., Dunai, T.J., 2008. A complete and easily accessible means of calculating surface exposure ages or erosion rates from ^{10}Be and ^{26}Al measurements. Quat. Geochronol. 4, 93–107.
Ballantyne, C.K., Stone, J.O., 2012. Did large ice caps persist on low ground in north-west Scotland during the Lateglacial Interstade? J. Quat. Sci. 27, 297–306.
Bevington, P., Robinson, D., 1992. Data Reduction and Error Analysis for the Physical Sciences. WCB McGraw Hill.
Bondevik, S., Mangerud, J., Birks, H.H., Gulliksen, S., Reimer, P., 2006. Changes in North Atlantic radiocarbon reservoir ages during the Allerød and Younger Dryas. Science 312, 1514–1517.
Borchers, B., Marrero, S., Balco, G., Caffee, M., Goehring, B., Lifton, N., Nishiizumi, K., Phillips, F., Schaefer, J., Stone, J., 2016. Geological calibration of spallation production rates in the CRONUS-Earth project. Quat. Geochronol. 31, 188–198.
Braucher, R., Bourlès, D., Merchel, S., Vidal Romani, J., Fernadez-Mosquera, D., Marti, K.,

Léanni, L., Chauvet, F., Arnold, M., Aumaître, G., Keddadouche, K., 2013. Determination of muon attenuation lengths in depth profiles from in situ produced cosmogenic nuclides. Nucl. Instrum. Methods Phys. Res. Sect. B Beam Interact. Mater. Atoms 294, 484–490.
Broecker, W.S., 2006. Abrupt climate change revisited. Global Planet. Change 54, 211–215.
Bromley, G., Putnam, A., Borns, H., Lowell, T., Sandford, T., Barrell, D., 2018. Interstadial rise and Younger Dryas demise of Scotland's last ice fields. Paleoceanography and Paleoclimatology 33, 412–429.
Bromley, G.R.M., Putnam, A.E., Lowell, T.V., Hall, B.L., Schaefer, J.M., 2016. Comment on 'was Scotland deglaciated during the Younger Dryas?' by Small and Fabel (2016). Quat. Sci. Rev. 152, 203–206.
Bromley, G.R.M., Putnam, A.E., Rademaker, K.M., Lowell, T.V., Schaefer, J.M., Hall, B.L., Winckler, G., Birkel, S.D., Borns, H.W., 2014. Younger Dryas deglaciation of Scotland driven by warming summers. Proc. Natl. Acad. Sci. Unit. States Am. 111, 6215–6219.
Browne, M.A.E., Graham, D.K., 1981. Glaciomarine deposits of the Loch Lomond stade glacier in the Vale of Leven between Dumbarton and Balloch, west-central Scotland. Quat. Newsl. 34, 1–7.
Browne, M.A.E., McMillan, A.A., Hall, I.H.S., 1983. Blocks of marine clay in till near Helensburgh, Strathclyde. Scot. J. Geol. 19, 321–325.
Buizert, C., Gkinis, V., Severinghaus, J.P., He, F., Lacavalier, B.S., Kindler, P., Leuenberger, M., Carlson, A.E., Vinther, B., Masson-Delmotte, V., White, J.W.C., Liu, Z., Otto-Bliesner, B., Brook, E.J., 2014. Greenland temperature response to climate forcing during the last deglaciation. Science 345, 1177–1180.
Chmeleff, J., von Blanckenburg, F., Kossert, K., Jakob, D., 2010. Determination of the ^{10}Be half-life by multicollector ICP-MS and liquid scintillation counting. Nucl. Instrum. Methods Phys. Res. Sect. B Beam Interact. Mater. Atoms 268, 192–199.
Claude, A., Ivy-Ochs, S., Kober, F., Antognini, M., Salcher, B., Kubik, P.W., 2014. The Chironico Landslide (Valle Leventina, southern Swiss Alps): age and evolution. Swiss J. Geosci. https://doi.org/10.1007/s000015-000014-000170-z.
Denton, G.H., Alley, R.B., Comer, G.C., Broecker, W.S., 2005. The role of seasonality in abrupt climate change. Quat. Sci. Rev. 24, 1159–1182.
Goehring, B.M., Kurz, M.D., Balco, G., Schaefer, J.M., Licciardi, J.M., Lifton, N., 2010. A reevaluation of in situ cosmogenic ^{3}He production rates. Quat. Geochronol. https://doi.org/10.1016/j.quageo.2010.03.001.
Goehring, B.M., Lohne, Ø.S., Mangerud, J., Svendsen, J.I., Gyllencreutz, R., Schaefer, J.M., Finkel, R., 2012. Late Glacial and Holocene ^{10}Be production rates for western Norway. J. Quat. Sci. 27, 89–96.
Golledge, N.R., 2007. An ice cap landsystem for palaeoglaciological reconstructions: characterizing the Younger Dryas in western Scotland. Quat. Sci. Rev. 26, 213–229.
Golledge, N.R., 2010. Glaciation of Scotland during the Younger Dryas stadial: a review. J. Quat. Sci. 25, 550–566.
Golledge, N.R., Fabel, D., Everest, J.D., Freeman, S., Binnie, S., 2007. First cosmogenic ^{10}Be age constraint on the timing of Younger Dryas glaciation and ice cap thickness, western Scottish Highlands. J. Quat. Sci. 22, 785–791.
Gray, J.M., Brooks, C.L., 1972. The Loch Lomond readvance moraines of Mull and Menteith. Scot. J. Geol. 8, 95–103.
Heisinger, B., Lal, D., Jull, A.J.T., Kubik, P., Ivy-Ochs, S., Knie, K., Nolte, E., 2002a. Production of selected cosmogenic radionuclides by muons: 2. Capture of negative muons. Earth Planet Sci. Lett. 200, 357–369.
Heisinger, B., Lal, D., Jull, A.J.T., Kubik, P., Ivy-Ochs, S., Neumaier, S., Knie, K., Lazarev, V., Nolte, E., 2002b. Production of selected cosmogenic radionuclides by muons: 1. Fast muons. Earth Planet Sci. Lett. 200, 345–355.
Heyman, J., 2014. Paleoglaciation of the Tibetan Plateau and surrounding mountains based on exposure ages and ELA depression estimates. Quat. Sci. Rev. 91, 30–41.
Jull, A.J.T., Scott, E.M., Bierman, P., 2015. The CRONUS-Earth inter-comparison for cosmogenic isotope analysis. Quat. Geochronol. 26, 3–10.
Kaplan, M.R., Strelin, J.A., Schaefer, J.M., Denton, G.H., Finkel, R.C., Schwartz, R., Putnam, A.E., Vandergoes, M.J., Goehring, B.M., Travis, S.G., 2011. In-situ cosmogenic ^{10}Be production rate at Lago Argentino, Patagonia: implications for late-glacial climate chronology. Earth Planet Sci. Lett. 309, 21–32.
Kelly, M.A., 2003. The Late Würmian Age in the Western Swiss Alps - Last Glacial Maximum (LGM) Ice-surface Reconstruction and ^{10}Be Dating of Late-glacial Features. University of Bern, pp. 105.
Kelly, M.A., Lowell, T.V., Applegate, P.J., Phillips, F.M., Schaefer, J.M., Smith, C.A., Kim, H., Leonard, K.C., Hudson, A.M., 2015. A locally calibrated, late glacial ^{10}Be production rate from a low-latitude, high-altitude site in the Peruvian Andes. Quat. Geochronol. 26, 70–85.
Kohl, C.P., Nishiizumi, K., 1992. Chemical isolation of quartz for measurement of in-situ -produced cosmogenic nuclides. Geochem. Cosmochim. Acta 56, 3583–3587.
Korschinek, G., Bergmaier, A., Dillmann, I., Faestermann, T., Gerstmann, U., Knie, K., von Gostomski, C.L., Maiti, M., Poutivtsev, M., Remmert, A., Rugel, G., Wallner, A., 2009. Determination of the ^{10}Be half-life by HI-IRD and liquid scintillation counting. Geochem. Cosmochim. Acta 73, A685.
Lal, D., 1991. Cosmic-ray labeling of erosion surfaces: in situ nuclide production rates and erosion models. Earth Planet Sci. Lett. 104, 424–439.
Lambeck, K., 1991. Glacial rebound and sea-level change in the British Isles. Terra. Nova 3, 379–389.
Lifton, N., Bieber, J., Clem, J., Duldig, M., Evenson, P., Humble, J., Pyle, R., 2005. Addressing solar modulation and long-term uncertainties in scaling secondary cosmic rays for in situ cosmogenic nuclide applications. Earth Planet Sci. Lett. 239, 140–161.
Lifton, N., Sato, T., Dunai, T.J., 2014. Scaling in situ cosmogenic nuclide production rates using analytical approximations to atmospheric cosmic-ray fluxes. Earth Planet Sci. Lett. 386, 149–160.
Lifton, N., Smart, B., Shea, M., 2008. Scaling time-integrated in situ cosmogenic nuclide production rates using a continuous geomagnetic model. Earth Planet Sci. Lett. 268, 190–201.
Lowe, J.J., 1982. Three flandrian pollen profiles from the Teith valley, Perthshire, Scotland. New Phytol. 90, 371–385.
Lowe, J.J., Walker, M.J.C., 1976. Radiocarbon dates and deglaciation of Rannoch Moor, Scotland. Nature 264, 632.
Mackintosh, A.N., Anderson, B.M., Pierrehumbert, R.T., 2017. Reconstructing climate from glaciers. Annu. Rev. Earth Planet Sci. 45, 649–680.
MacLeod, A., Matthews, I.P., Lowe, J.J., Palmer, A.P., Albert, P.G., 2015. A second tephra isochron for the Younger Dryas period in northern Europe: the Abernethy Tephra. Quat. Geochronol. 28, 1–11.
Martin, L.C.P., Blard, P.-H., Lavé, J., Braucher, R., Lupker, M., Condom, T., Charreau, J., Mariotti, V., Team, A.S.T.E.R., Davy, E., 2015. In situ ^{10}Be production rate in the High Tropical Andes. Quat. Geochronol. 30A, 54–68.
Nishiizumi, K., Imamura, M., Caffee, M.W., Southon, J.R., Finkel, R.C., McAninch, J., 2007. Absolute calibration of ^{10}Be AMS standards. Nucl. Instrum. Methods Phys. Res. B 258, 403–413.
Oerlemans, J., 2005. Extracting a climate signal from 169 glacier records. Science 308, 675–677.
Ordnance Survey, 2015. Rannoch Moor & Ben Alder, Sheet 385. Ordnance Survey (Explorer Series), Southampton.
Palmer, A.P., Rose, J., Lowe, J.J., MacLeod, A., 2010. Annually resolved events of Younger Dryas glaciation in Lochaber (Glen Roy and Glen Spean), western Scottish Highlands. J. Quat. Sci. 25, 581–596.
Peacock, J.D., 1971. Marine shell radiocarbon dates and the chronology of deglaciation in western Scotland. Nat. Phys. Sci. (Lond.) 230, 43.
Phillips, F.M., 2015. Preface – the CRONUS-EARTH volume. Quat. Geochronol. 26, 1–2.
Phillips, F.M., Argento, D.C., Balco, G., Caffee, M.W., Clem, J., Dunai, T.J., Finkel, R., Goehring, B., Gosse, J.C., Hudson, A.M., Jull, A.J.T., Kelly, M.A., Kurz, M., Lal, D., Lifton, N., Marrero, S.M., Nishiizumi, K., Reedy, R.C., Schaefer, J., Stone, J.O.H., Swanson, T., Zreda, M.G., 2016. The CRONUS-Earth Project: a synthesis. Quat. Geochronol. 31, 119–154.
Pigati, J.S., Lifton, N.A., 2004. Geomagnetic effects on time-integrated cosmogenic nuclide production with emphasis on in situ ^{14}C and ^{10}Be. Earth Planet Sci. Lett. 226, 193–205.
Putnam, A.E., Denton, G.H., Schaefer, J.M., Barrell, D.J.A., Andersen, B.G., Finkel, R., Schwartz, R., Doughty, A.M., Kaplan, M., Schlüchter, C., 2010a. Glacier advance in southern middle latitudes during the Antarctic Cold Reversal. Nat. Geosci. 3, 700–704.
Putnam, A.E., Schaefer, J.M., Barrell, D.J.A., Vandergoes, M., Denton, G.H., Kaplan, M.R., Schwartz, R., Finkel, R.C., Goehring, B.M., Kelley, S.E., 2010b. In situ cosmogenic ^{10}Be production-rate calibration from the Southern Alps, New Zealand. Quat. Geochronol. 5, 392–409.
Rasmussen, S.O., Andersen, K.K., Svensson, A.M., Steffensen, J.P., Vinther, B.M., Clausen, H.B., Siggaard-Andersen, M.-L., Johnsen, S.J., Larsen, L.B., Dahl-Jensen, D., Bigler, M., Röthlisberger, R., Fischer, H., Goto-Azuma, K., Hansson, M.E., Ruth, U., 2006. A new Greenland ice core chronology for the last glacial termination. J. Geophys. Res. 111, D06102.
Reimer, P.J., Bard, E., Bayliss, A., Beck, J.W., Blackwell, P.G., Bronk Ramsay, C., Buck, C.E., Cheng, H., Edwards, R.L., Friedrich, M., Grootes, P., Guilderson, T.P., Haflidason, H., Hajdas, I., Hatté, C., Heaton, T.J., Hoffmann, D.L., Hogg, A.G., Hughen, K.A., Kaiser, K.F., Kromer, B., Manning, S.W., Niu, M., Reimer, R.W., Richards, D.A., Scott, E.M., Southon, J.R., Staff, R.A., Turney, C.S.M., van der Plicht, J., 2013. INTCAL13 and MARINE13 radiocarbon age calibration curves 0-50,000 years cal BP. Radiocarbon 55, 1869–1887.
Rose, J., 1980. Quaternary Research Association Glasgow Region Field Guide. Quaternary Research Association, Cambridge, pp. 25–37.
Rupper, S., Roe, G., 2008. Glacier changes and regional climate: a mass and energy balance approach. J. Clim. 21, 5384–5401.
Schaefer, J.M., Denton, G.H., Kaplan, M., Putnam, A., Finkel, R.C., Barrell, D.J.A., Andersen, B.G., Schwartz, R., Mackintosh, A., Chinn, T., Schlüchter, C., 2009. High-frequency Holocene glacier fluctuations in New Zealand differ from the northern signature. Science 324, 622–625.
Schenk, F., Väliranta, M., Muschitiello, F., Tarasov, L., Heikkilä, M., Björck, S., Brandefelt, J., Johansson, A.V., Näslund, J.-O., Wohlfarth, B., 2018. Warm summers during the Younger Dryas cold reversal. Nat. Commun. 9, 1634.
Sissons, J.B., 1967. Glacial stages and radiocarbon dates in Scotland. Scot. J. Geol. 3, 375–381.
Sissons, J.B., 1976. The Geomorphology of the British Isles: Scotland. Methuen, London.
Sissons, J.B., 1978. The parallel roads of Glen Roy and adjacent glens, Scotland. Boreas 7, 229–244.
Small, D., Fabel, D., 2015. A Lateglacial ^{10}Be production rate from glacial lake shorelines in Scotland. J. Quat. Sci. 30, 509–513.
Small, D., Fabel, D., 2016a. Response to Bromley et al. "Comment on 'Was Scotland deglaciated during the Younger Dryas?' By Small and Fabel (2016)". Quat. Sci. Rev. 152, 206–208.
Small, D., Fabel, D., 2016b. Was Scotland deglaciated during the Younger Dryas? Quat. Sci. Rev. 145, 259–263.
Stockamp, J., Bishop, P., Li, Z., Petrie, E.J., Hansom, J., Rennie, A., 2016. State-of-the-art in studies of glacial isostatic adjustment for the British Isles: a literature review. Earth and Environmental Science Transactions of the Royal Society of Edinburgh 106, 145–170.
Stone, J.O., 2000. Air pressure and cosmogenic isotope production. J. Geophys. Res. 105, 23753–23759.
Stone, J.O., Ballantyne, C.K., Keith Fifield, L., 1998. Exposure dating and validation of periglacial weathering limits, northwest Scotland. Geology 26, 587–590.
Strelin, J.A., Denton, G.H., Vandergoes, M.J., Ninnemann, U.S., Putnam, A.E., 2011.

Radiocarbon chronology of the late-glacial Puerto Bandera moraines, Southern Patagonian Icefield, Argentina. Quat. Sci. Rev. 30, 2551–2569.

Stroeven, A.P., Heyman, J., Fabel, D., Björck, S., Caffee, M.W., Fredin, O., Harbor, J.M., 2015. A new Scandinavian reference ^{10}Be production rate. Quat. Geochronol. 29, 104–115.

Thorp, P.W., 1984. The Glacial Geomorphology of Part of the Western Grampians of Scotland with Especial Reference to the Limits of the Loch Lomond Advance. City of London Polytechnic.

Thorp, P.W., 1986. A mountain icefield of Loch Lomond stadial age, western Grampians, Scotland. Boreas 15, 83–97.

Uppala, S.M., KÅllberg, P.W., Simmons, A.J., Andrae, U., Bechtold, V.D.C., Fiorino, M., Gibson, J.K., Haseler, J., Hernandez, A., Kelly, G.A., Li, X., Onogi, K., Saarinen, S., Sokka, N., Allan, R.P., Andersson, E., Arpe, K., Balmaseda, M.A., Beljaars, A.C.M., Berg, L.V.D., Bidlot, J., Bormann, N., Caires, S., Chevallier, F., Dethof, A., Dragosavac, M., Fisher, M., Fuentes, M., Hagemann, S., Hólm, E., Hoskins, B.J., Isaksen, L., Janssen, P.A.E.M., Jenne, R., Mcnally, A.P., Mahfouf, J.F., Morcrette, J.J., Rayner, N.A., Saunders, R.W., Simon, P., Sterl, A., Trenberth, K.E., Untch, A., Vasiljevic, D., Viterbo, P., Woollen, J., 2005. The ERA-40 re-analysis. Q. J. R. Meteorol. Soc. 131, 2961–3012.

Walker, M.J.C., Lowe, J.J., 1977. Postglacial environmental history of Rannoch Moor, Scotland. I. Three Pollen diagrams from the Kingshouse Area. J. Biogeogr. 4, 333–351.

Walker, M.J.C., Lowe, J.J., 1982. Lateglacial and early flandrian chronology of the Isle of Mull, Scotland. Nature 296, 558.

Walker, M.J.C., Lowe, J.J., 1979. Postglacial environmental history of Rannoch Moor, Scotland. II. Pollen diagrams and radiocarbon dates from the Rannoch station and Corrour areas. J. Biogeogr. 6, 349–362.

Young, N.E., Schaefer, J.M., Briner, J.P., Goehring, B.M., 2013. A ^{10}Be production-rate calibration for the Arctic. J. Quat. Sci. 28, 515–526.

Zemp, M., Frey, H., Gärtner-Roer, I., Nussbaumer, S.U., Hoelzle, M., Paul, F., Haeberli, W., Denzinger, F., Ahlstrøm, A.P., Anderson, B., Bajracharya, S., Baroni, C., Braun, L.N., Cáceres, B.E., Casassa, G., Cobos, G., Dávila, L.R., Delgado Granados, H., Demuth, M.N., Espizua, L., Fischer, A., Fujita, K., Gadek, B., Ghazanfar, A., Hagen, J.O., Holmlund, P., Karimi, N., Li, Z., Pelto, M., Pitte, P., Popovnin, V.V., Portocarrero, C.A., Prinz, R., Sangewar, C.V., Severskiy, I., Sigurðsson, O., Soruco, A., Usubaliev, R., Vincent, C., 2015. Historically unprecedented global glacier decline in the early 21st century. J. Glaciol. 61, 745–762.